การรับแรงร่วมกันระหว่างแผ่นพื้นวงกลมกับตัวกลางโพโรอิลาสติกหลายชั้น

นายสงกรานต์ ศิริเดชาชัย

วิทยานิพนธ์นี้เป็นส่วนหนึ่งของการศึกษาตามหลักสูตรปริญญาวิศวกรรมศาสตรมหาบัณฑิต
สาขาวิชาวิศวกรรมโยธา ภาควิชาวิศวกรรมโยธา
คณะวิศวกรรมศาสตร์ จุฬาลงกรณ์มหาวิทยาลัย
ปีการศึกษา 2544

ISBN 974-03-1446-5

THE INTERACTION BETWEEN A CIRCULAR PLATE AND A MULTI-LAYERED POROELASTIC HALF-SPACE

Mr. Songkran Siridejachai

A Thesis Submitted in Partial Fulfillment of the Requirements
for the Degree of Master of Engineering in Civil Engineering

Department of Civil Engineering
Faculty of Engineering
Chulalongkorn University

Academic Year 2001
ISBN 974-03-1446-5

Thesis Title	The Interaction between a Circular Plate and a Multi-layered Poroelastic Half-space
By	Mr. Songkran Siridejachai
Field of Study	Civil Engineering
Thesis Advisor	Asst. Prof. Dr. Teerapong Senjuntichai

Accepted by the Faculty of Engineering, Chulalongkorn University in Partial Fulfillment of the Requirements for the Master's Degree

..... Dean of Faculty of Engineering

(Professor Somsak Panyakeow, D.Eng.)

THESIS COMMITTEE

..... Chairman

(Associate Professor Suthum Suriyamongkol, D.Eng.)

..... Thesis Advisor

(Assistant Professor Teerapong Senjuntichai, Ph.D.)

..... Member

(Assistant Professor Boonchai Ukritchon, Sc.D.)

สงกรานต์ ศิริเดชาชัย : การรับแรงร่วมกันระหว่างแผ่นพื้นวงกลมกับตัวกลางโพโรอิลาสติกหลายชั้น (The Interaction between a Circular Plate and a Multi-layered Poroelastic Half-space) อ.ที่ปรึกษา : ผศ.ดร.ธีรพงศ์ เสนจันทร์ฒิไชย, 58 หน้า. ISBN 974-03-1446-5

วิทยานิพนธ์ฉบับนี้เป็นการศึกษาปัญหาการรับแรงร่วมกันระหว่างแผ่นพื้นวงกลมกับตัวกลางโพโรอิลาสติกหลายชั้น ระบบที่พิจารณาประกอบด้วยแผ่นพื้นวงกลมรับแรงกระทำแบบสมมาตรกับรอบแกนชนิดแรงเป็นจุดและชนิดแรงกระจายสม่ำเสมอ โดยแผ่นพื้นนี้จะฝังอยู่ในตัวกลางดังกล่าว ตัวกลางแต่ละชั้นมีความหนาและคุณสมบัติของวัสดุแตกต่างกัน สมการแสดงการทรุดตัวของแผ่นพื้น จะสมมติให้อยู่ในรูปอนุกรมกำลังของตัวแปรรัศมี โดยมีตัวแปรไม่รู้ค่าประกอบอยู่ในสมการการทรุดตัวด้วย พลังงานศักย์รวมของระบบจะประกอบไปด้วยส่วนของแผ่นพื้น ตัวกลางหลายชั้นและส่วนของแรงกระทำ ตัวแปรไม่รู้ค่าสามารถหาได้โดยใช้หลักการของพลังงานศักย์รวมต่ำสุด พฤติกรรมของแผ่นพื้นคือค่าการทรุดตัว ค่าโมเมนต์ดัด ค่าแรงเฉือน ค่าแรงต้านทานลัพธ์ และค่าแรงดันน้ำที่เกิดขึ้น สามารถทราบได้โดยการแทนค่าตัวแปรไม่รู้ค่ากลับเข้าไปในสมการแสดงการทรุดตัวของแผ่นพื้นที่ถูกสมมติขึ้น เมื่อนำผลลัพธ์จากการวิจัยครั้งนี้ไปเปรียบเทียบกับการศึกษาในอดีต พบว่ามีความสอดคล้องกัน นอกจากนั้นยังได้นำเสนออิทธิพลของตัวแปรต่างๆ ที่มีผลต่อพฤติกรรมของแผ่นพื้นวงกลม เช่น ความแข็งของแผ่นพื้น ชนิดของแรงกระทำ ระยะความลึกที่แผ่นพื้นฝังอยู่ในตัวกลาง การทรุดตัวเมื่อตัวกลางวางอยู่บนชั้นหินแข็ง

ภาควิชา วิศวกรรมโยธา ลายมือชื่อนิสิต .....

สาขาวิชา วิศวกรรมโยธา ลายมือชื่ออาจารย์ที่ปรึกษา.....

ปีการศึกษา 2544

4170550521 : MAJOR CIVIL ENGINEERING

KEY WORD : ELASTIC PLATE / MULTI-LAYERED MEDIA / SOIL-STRUCTURE INTERACTION / POROELASTICITY

SONGKARN SIRIDEJACHAI : THE INTERACTION BETWEEN A CIRCULAR PLATE AND A MULTI-LAYERED POROELASTIC HALF-SPACE, THESIS ADVISOR : ASST. PROF. DR. TEERAPONG SENJUNTICHAI, 58 pp. ISBN 974-03-1446-5.

This thesis is concerned with the interaction between an axisymmetrically loaded circular plate buried in a multi-layered poroelastic half-space by employing an energy method. The assumed deflected shape is in the form of a set of undetermined constants. The total potential energy functional consists of the strain energy of multi-layered media, the strain energy of the circular plate and the potential energy of the applied loads. The unknown constants are obtained from a linearly independent algebraic equation system obtained from the minimization of the total potential energy functional. The accuracy of the present scheme is confirmed by comparing with the existing results. Selected numerical results for displacement and bending moment of a plate as well as stresses and pore pressure in a multi-layered poroelastic half-space are presented to portray the influence of plate stiffness, types of loading and poroelastic material properties on the interaction problem.

Department ..... Civil Engineering ..... Student's signature.....

Field of study..... Civil Engineering ..... Advisor's signature.....

Academic year 2001

ACKNOWLEDGEMENTS

The author is greatly indebted to his advisor Assistant Professor Dr.Teerapong Senjuntichai for his continuous guidance suggestions, encouragement and help which makes this thesis possible. He would also like to express his profound gratitude to Associate Professor Dr.Suthum Suriyamongkol as a chairman and Assistant Professor Dr.Boonchai Ukritchon for serving as a member of the thesis committee and giving the worthy recommendations. Thanks are also due to Professor R.K.N.D. Rajapakse from University of British Columbia, Canada, for his invaluable comment on this thesis.

Finally, a special debt of gratitude is offered to author's parents for the many favor they have made to his educational objectives.

Songkran Siridejachai

CONTENTS

Abstract (Thai) iv

Abstract (English) v

Acknowledgements vi

Contents vii

List of tables ix

List of figures x

List of symbols xiii

Chapter I Introduction 1

1.1 General 1

1.2 Objective and scope of present study 1

1.3 Basic assumptions 2

Chapter II Literature reviews 3

Chapter III Theoretical considerations 7

3.1 Basic equations 7

3.2 Stiffness matrices 9

3.3 Global stiffness matrices 10

3.4 Boundary conditions of multi-layered half-space 10

3.5 Strain energy of circular plate 11

3.6 Strain energy of multi-layered poroelastic medium 13

3.7 Variational formulation of interaction problem 14

Chapter IV Numerical solutions 16

4.1 Numerical scheme 16

4.2 Comparison with existing solutions 16

4.3 Numerical results and discussion 20

Chapter V Conclusions 24

References 53

Appendix 57

Biography 58

LIST OF TABLES

Table		Page
1	Convergence of solution, W*(0), with NT and M for a centrally loaded plate compare with Rajapakse(1988).....	17
2	Convergence of solution, M_r*(0.5a), with N and M for a centrally loaded plate compare with Rajapakse(1988).	17
3	Comparison of dimensionless displacements, $a\mu w/P_o$, of a rigid circular plate with Yue and Selvadurai (1995).....	25
4(a)	Comparison of dimensionless radial bending moment with Brown (1969).....	26
4(b)	Comparison of dimensionless tangential bending moment with Brown (1969).....	26

LIST OF FIGURES

Figure		Page
1	Geometry of plate-multi-layered poroelastic medium system	5
2	(a) Forces and displacements of n^{th} layer. (b) Free body diagram of the interaction problem. (c) Model used to discretize traction into unit annular ring load	6
3	Comparison between degree of consolidation settlement of a centrally loaded rigid plate from present study (H/a = 0.0, ν = 0.0, ν_u = 0.5)	18
4	Comparison of variation of normalized central deflection of a uniformly loaded plate with relative rigidity K_r and degree of non-homogeneity, m*, (from present study with results from Rajapakse and Selvadurai, 1991)	27
5	Comparison of variation of normalized central deflection of anchor plates with relative rigidity K_r and depth of embedment for a soil with μ_o = 0, (from present study with results from Rajapakse and Selvadurai, 1991)	27
6	Comparison of axial displacement of the rigid plate	28
7	Effect of Poisson's ratios and surface drainage on the consolidation induced axial displacement of the rigid punch	29
8	Geometry of problem 1	30
9	Variation of (a) dimensionless central displacement W*(0) and (b) radial bending moment M_r*(0.01a) of a centrally loaded plate with time and drainage boundary condition	31

10 Variation of dimensionless central displacement W*(0) of a centrally loaded plate with time and relative rigidity parameter K_r 32

11 Variation of radial bending moment M_r*(0.01a) of a centrally loaded plate with time and relative rigidity paraemter K_r 33

12 Variation of displacement profile of a centrally loaded plate (K_r = 1.0) with times .. 34

13 Variation of displacement profile of a centrally loaded rigid plate (K_r = 10000) with times 35

14 Variation of (a) displacement profile and (b) radial bending moment profile of a centrally loaded plate with relative rigidity K_r 36

15 Variation of (a) dimensionless central displacement W*(0) and (b) radial bending moment M_r*(0) of a uniformly loaded plate with time and drainage boundary condition 37

16 Variation of dimensionless central displacement W*(0) of a uniformly loaded plate with time and relative rigidity parameter K_r 38

17 Variation of dimensionless radial bending moment M_r*(0) of a uniformly loaded plate with time and relative rigidity parameter K_r 39

18 Variation of displacement profile of a uniformly loaded plate (K_r = 1.0) with times. 40

19 Variation of displacement profile of a uniformly loaded rigid plate (K_r = 10000) with times 41

20 Variation of (a) displacement profile and (b) radial bending moment profile of a uniformly loaded plate with relative rigidity K_r 42

21 Variation of contact stress profile of (a) a centrally loaded plate and (b) a uniformly loaded plate with relative rigidity K_r 43

22 (a) Pore pressure history beneath the plate (z = a, r = 0). (b) Final solution of the contact stress profiles at the bottom surface of the first layer and the top surface of the second layer due to a circular plate subjected a uniform load 44

23 Geometry of problem 2 45

24 Variation of dimensionless central displacement W*(0) of a centrally loaded plate (K_r = 1.0) with time and depth of the 3rd layer 46

25 Variation of radial bending moment at r = 0.01a of a centrally loaded plate (K_r = 1.0) with time and depth of the 3rd layer 47

26 Geometry of problem 3 48

27 Variation of dimensionless central displacement of a uniformly loaded plate (K_r = 2.0) with time and thickness of the 2nd layer 49

28 Variation of dimensionless radial bending moment M_r*(0) of a uniformly loaded plate (K_r = 2.0) with time and thickness of the 2nd layer 50

29 Variation of final solution of (a) displacement profile and (b) radial bending moment profile of a uniformly loaded plate with depth of the 2nd layer 51

30 Variation of (a) dimensionless central displacement W*(0) and (b) dimensionless radial bending moment M_r*(0) of a uniformly loaded plate with relative rigidity parameter K_r and thickness of the 2nd layer 52

LIST OF SYMBOLS

$[\ ]$	rectangular or square matirx
$[\ ]^T$	matrix transpose
$\{\ \}$	column vector
$\langle\ \rangle$	row vector
a	radius of circular elastic plate
B	Skempton's pore pressure coefficient
$c^{(n)}$	consolidation coefficient for the n^{th} layer
E_p	modulus of elasticity of plate
$E_s^{(n)}$	modulus of elasticity of the n^{th} layer
$F^{(n)}$	generalized force vector for the n^{th} layer
i, j, k, m, n	general indices
J_m	Bessel function of the first kind of order m^{th}
$K^{(n)}$	stiffness matrix for the n^{th} layer
K_r	relative rigidity parameter
M	number of elements used for discretization the circular plate
M_r, M_t	radial and tangential bending moments per unit distance
NT	number of generalized co-ordinates in assumed displacement function
P_o	central vertical force acting on the plate
p	excess pore fluid pressure
q_o	uniform distribute load
r	radial co-ordinate
Δr	width of ring element
s	Laplace transform parameter
$T^{(n)}$	vector of generalized tractions and fluid flow for the n^{th} layer
t	time variable
$U^{(n)}$	generalized displacement vector for the n^{th} layer
U_h	strain energy of multi-layered poroelastic half-space
U_p	straing energy of circular elastic plate
u_i	displacement of solid matrix in the i-direction
W*	normalized displacement of circular elastic plate

$w(r)$	displacement of circular elastic plate
z	vertical co-ordinate
α_n	generalized co-ordinates
δ_{ij}	Kronecker delta
ε	dilatation of solid matrix
ε_{ij}	strain component of solid matrix
$\kappa^{(n)}$	permeability for the n^{th} layer
$\mu^{(n)}$	shear modulus of poroelastic material for the n^{th} layer
$\nu^{(n)}$	drained Poisson's ratio for the n^{th} layer
ν_p	Poisson's ratio of plate
$\nu_u^{(n)}$	undrained Poisson's ratio for the n^{th} layer
σ_{ij}	stress component of bulk material
ξ	Hankel transform parameter
ζ	the variation of fluid volume per unit reference volume

CHAPTER I

INTRODUCTION

1.1 GENERAL

The classical problem of determining stress and displacement distribution due to the interaction between a plate and a half-space has been a subject of interest in civil engineering since the pioneer work by Boussinesq (Boussinesq, 1885) due to its application in the analysis and design of foundations. A variety of analytical, semi-analytical and numerical methods have been employed to analyze the plate-half-space interaction problem. The deformations as well as the bending moment in plate not only depend on the flexibility of the plate, but also on the half-space behavior. The actual behavior of the half-space is very complex and several attempts have been made to develop a number of idealised models to represent the half-space.

One of the most widely used models for soil is the elastic continuum in which the soil is assumed to be homogeneous or nonhomogeneous isotropic elastic half-space. Several works on plate-half-space problem have been presented (Butterfield and Banerjee, 1971; Carrier and Christian, 1973; Chakravorty and Ghosh, 1975; Hemsley, 1987; Melerski, 1997, etc.). However, those researchers did not take into account the realistic character of soil, which is solid skeleton filled with water, commonly known as poroelastic effect. In this thesis, the interaction between a circular elastic plate and a multi-layered poroelastic half-space under axisymmetric loading is considered.

1.2 OBJECTIVE AND SCOPE OF PRESENT STUDY

The objective of this research is to investigate the interaction between a circular elastic plate and multi-layered poroelastic half-space by following a variational method developed by Rajapakse (1988) and the exact stiffnes matrix scheme proposed by Senjuntichai and Rajapakse (1995). The study is concentrated on the mechanical behavior of the plate-half-space system. The contact surface between plate and medium is considered as either fully permeable or impermeable and assumed to be smooth. The applied loading is restricted only to the axisymmetric case. A computer program is developed to analyze the behavior of contact problem, i.e. displacement, bending moment, contact stress, pore pressure, etc. A variety of parametric study is carried out, i.e. the influence of material properties, rigidity of plate, type of applied loading, etc.

1.3 BASIC ASSUMPTIONS

The following assumptions are employed in the present study

1.) Each layer of the multi-layered half-space is a homogeneous poroelastic material and governed by Biot's theory of poroelasticy and all layer interfaces are assumed to be perfectly bonded, i.e. no separation occur.

2.) The plate under consideration is resting on or buried in a multi-layer half-space and subjected to axisymmetric loading.

3.) The contact surface between the plate and the multi-layered poroelastic half-space is assumed to be smooth and either fully permeable or impermeable.

CHAPTER II

LITERATURE REVIEWS

The study of interaction between a circular elastic plate and the medium has useful applications in civil engineering. For example, the plate-elastic medium model can be used to simulate the working load response of surface or embedded foundations, circular columns or the shafts of water towers, anchor plates resisting uplift loads and theoretical modeling of some in-situ testing methods.

In the analysis, it is necessary to choose a suitable soil model for the foundation. Even in the elastic range, there are a number of proposed soil models. The simplest among them is the Winkler's model, in which the deformation of a surface point is directly proportional to the intensity of the vertical stress at the point, resulting in only one material parameter in the model equation. Although the Winkler's model is very simple and convenient in applications, the simulated result to the practice is not good. Another idealization assumes continuum behaviour of the soil, and the soil medium is thus represented by an elastic half-space. The basic solution for this model can be found in the work of Boussinesq (1855), who analyzed the problem of a semi-infinite homogeneous isotropic elastic solid subjected to a concentrated force that acts normal to the plane boundary. There are two models which have also been used in the analysis of plate-soil interaction problem, i.e. non-homogeneous elastic soil and poroelastic soil.

The characteristic of non-homogeneous elastic soil is its Young's modulus increases linearly with depth. Gibson (1967) presented a fundamental study on the response of a linearly non-homogeneous incompressible elastic soil subjected to a vertical load at the surface level and the several researchers have employed Gibson's soil model to analyze the interaction problem (e.g. Rajapakse and Selvadurai, 1991; Wang, Ni and Cheung, 2000). The theory of poroelasticity has its origin in the one-dimensional theory of soil consolidation proposed by Terzaghi (1923). Biot (1941) developed a general theory of three-dimensional consolidation of fluid-saturated porous elastic solids by adopting Terzaghi's concepts. Later, Rice and Cleary (1976) reformulated Biot's work in terms of material constants which are more easily identified. Over the last forty

years, Biot's theory has been the basis for analysis of a variety of geotechnical problems related to poroelastic regions.

A comprehensive review of elastic methods of analysis applied the present class of problems was presented by Selvadurai (1979). Pickett and McCormick (1951) analyzed the contact problem of circular/rectangular plates and the elastic foundation by employing double Fourier series techniques. Palmov (1960) and Popov (1971) solved the interaction problem by using integral equation methods. Brown (1969a, b) studied the interaction of a circular raft, subjected to an axisymmetrical load, resting on an isotropic elastic layer of finite thickness by making use of Burmister's solution for point loads (Burmister, 1956) and Sneddon's solution (Sneddon, 1951). Hooper (1974, 1975) used a total finite element method to solve the interaction of a circular raft bonded to elastic foundation and transversely isotropic medium. Rajapakse and Selvadurai (1991) investigated the response of circular footings and anchor plates in non-homogeneous elastic soils by using variational technique. Yue and Selvadurai (1995) considered an interaction between a rigid circular plate and a homogeneous poroelastic half-space by employing the integral transform techniques. Recently, Wang, et al. (2000) and Wang and Cheung (2001) used the Finite Element method to examine behaviour of a square plate resting on the non-homoegneous elastic half-space and on the cross-anisotropic foundation, respectively. The interaction of ring plate and a multi-layered transversely isotropic elastic half-space were also considered by Antony and Chandreshekhara (2000) by using FEM.

The present study is concerned with the analysis of the elastic circular plate/multi-layered poroelastic half-space system resisting axisymmetric load as shown in Figure 1. A variational solution scheme (Rajapakse, 1988) is presented in a matrix form. The displacement of the plate is represented by a power series of radial co-ordinate containing a set of generalized co-ordinates, together with a term corresponding to the particular solution of a centrally loaded circular plate. The strain energy of the plate is derived as a quadratic function of generalized co-ordinates.

The next step is to establish a total potential energy functional which consists of the strain energy of the plate, the strain energy of the half-space and the potential energy of the external loading. The minimization of the energy functional with respect to generalized co-ordinates yields a system of linear simultaneous equations. Numerical solution of the equation system yields the

values of the generalized co-ordinates for a system shown in Figure 1. Selected numerical results are presented to illustrate the convergence and numerical stability of the proposed variational formulation and the response of the elastic plate.

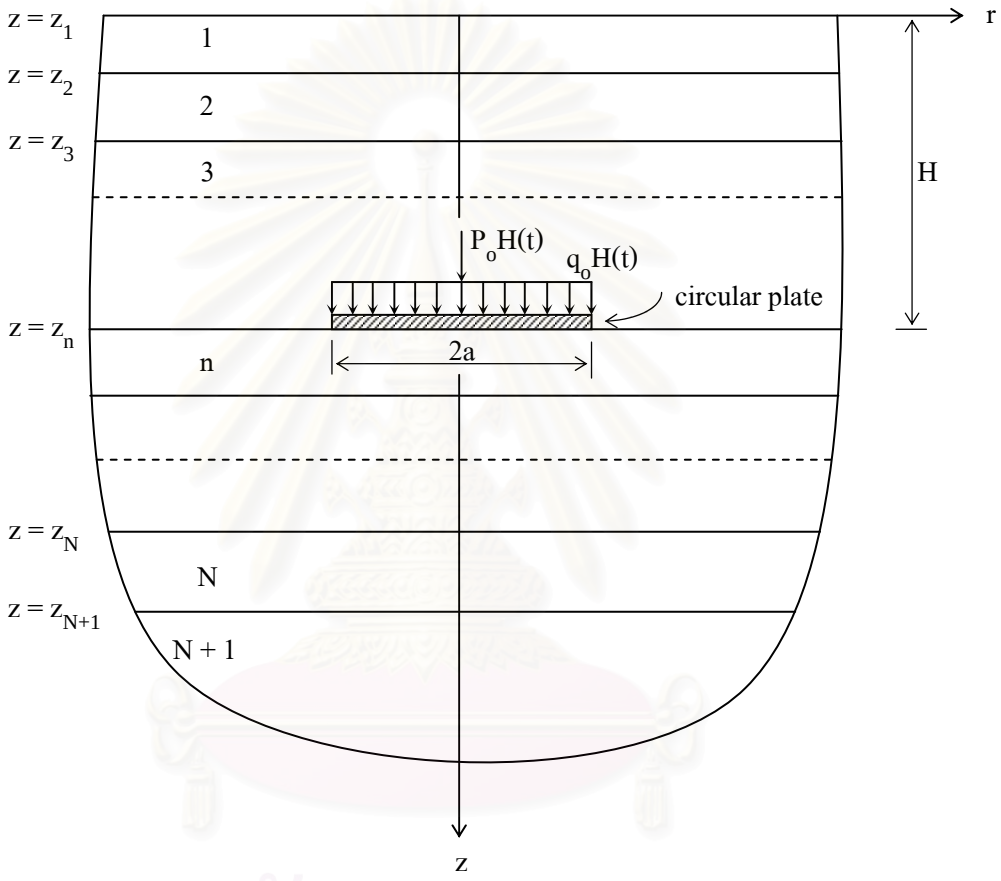

Figure 1. Geometry of plate-multi-layered poroelastic medium system

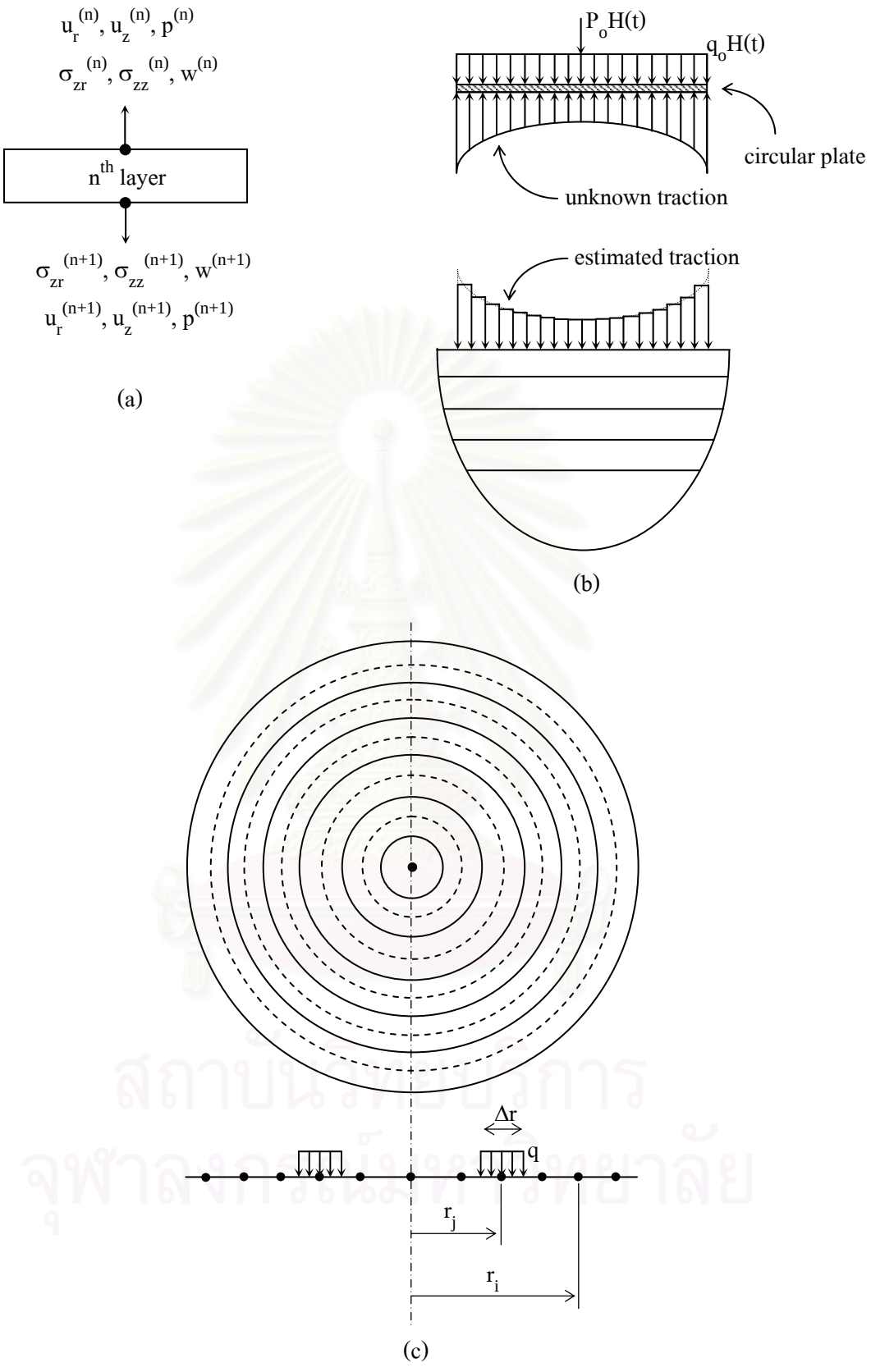

Figure 2. (a) Forces and displacements of n^{th} layer. (b) Free body diagram of the interaction problem. (c) Model used to discretize traction into unit annular ring load.

CHAPTER III

THEORETICAL CONSIDERATIONS

3.1 BASIC EQUATIONS

The quasi-static governing equations (Rice and Cleary, 1976) of a poroelastic medium for an axisymmetric problem can be expressed in cylindrical co-ordinate, (r, z), system and time, t, as

$$\nabla^2 u_r + \frac{1}{1-2\nu_u}\frac{\partial \varepsilon}{\partial r} - \frac{u_r}{r^2} - \frac{2B(1+\nu_u)}{3(1-2\nu_u)}\frac{\partial \zeta}{\partial r} = 0 \tag{1}$$

$$\nabla^2 u_z + \frac{1}{1-2\nu_u}\frac{\partial \varepsilon}{\partial z} - \frac{2B(1+\nu_u)}{3(1-2\nu_u)}\frac{\partial \zeta}{\partial z} = 0 \tag{2}$$

$$\nabla^2 \zeta = \frac{1}{c}\frac{\partial \zeta}{\partial t} \tag{3}$$

where

$$\nabla^2 = \frac{\partial^2}{\partial r^2} + \frac{1}{r}\frac{\partial}{\partial r} + \frac{\partial^2}{\partial z^2} \tag{4}$$

$$\varepsilon = \frac{\partial u_r}{\partial r} + \frac{u_r}{r} + \frac{\partial u_z}{\partial z} \tag{5}$$

$$c = \frac{2}{9}\frac{\mu\kappa B^2(1-\nu)(1+\nu_u)^2}{(1-\nu_u)(\nu_u-\nu)} \tag{6}$$

In which u_r and u_z are displacements in the r and z direction, respectively, and ζ denotes the variation of fluid volume per unit reference volume. The five material parameters in the above equations are the drained and undrained Poisson's ratios ν and ν_u, respectively; the shear modulus $\mu(> 0)$; Skempton's (1954) pore pressure coefficient B and $\kappa = k/\gamma_w$ where k is the coefficient of permeability, γ_w is the unit weight of pore fluid and $\kappa > 0$. It is noted that $0 \le B \le 1$ and $\nu \le \nu_u \le 0.5$ for all poroelastic materials. The limiting cases of a poroelastic solid with incompressible constituents and a dry elastic material are obtained when $\nu_u = 0.5$ and $B = 1$, and $B \to 0$, respectively.

The constitutive relations for a poroelastic material can be expressed by using standard indicial notations as

$$\sigma_{ij} = 2\mu\left(\varepsilon_{ij} + \frac{\nu}{1-2\nu}\delta_{ij}\varepsilon\right) - \frac{3(\nu_u-\nu)}{B(1-2\nu)(1+\nu_u)}\delta_{ij}p, \qquad i, j = r, z \tag{7}$$

In eqn (7), σ_{ij} and ε_{ij} denote the total stresses and strains component of the bulk material, respectively; ε is the dilatation of solid matrix which is defined in eqn (5); δ_{ij} is the Kronecker δ.

In addition, p is the excess pore fluid pressure (suction is considered negative) and can be expressed in terms of dilatation and variation of fluid volume as

$$\frac{p}{2\mu} = -\frac{B(1+\nu_u)}{3(1-2\nu_u)}\varepsilon + \frac{B^2(1-2\nu)(1+\nu_u)^2}{9(1-2\nu_u)(\nu_u-\nu)}\zeta \tag{8}$$

At this stage, it is convenient to nondimensionalize all quantities including the co−ordinate frame with respect to length and time by selecting the radius of a circular plate "a" as a unit length and "a^2/c" as a unit of time, respectively. All variables will be replace by appropriate nondimensional variables, but the previous notations will be used for convenience.

In the following manipulation, the integral transforms technique is used to solve the partial differential equations (1)-(3). The Laplace-Hankel transform (m^{th} order) of function $\phi(r, z, t)$ with respect to the variables t and r, respectively, is defined by (Sneddon, 1951)

$$\bar{\phi}(\xi, z, s) = \int_0^\infty \int_0^\infty \phi(r, z, t)\, e^{-st} J_m(\xi r)\, r\, dr\, dt \tag{9}$$

In eqn (9), s and ξ denote the Laplace and Hankel transform parameters respectively, and J_m denotes the Bessel function of the first kind of order m. The inverse relationship is given by

$$\phi(r, z, t) = \frac{1}{2\pi i}\int_{\omega-i\infty}^{\omega+i\infty}\int_0^\infty \bar{\phi}(\xi, z, s)\, e^{st} J_m(\xi r)\, \xi\, d\xi\, ds \tag{10}$$

where ω is greater than the real part of all singularities of $\bar{\phi}(\xi, z, s)$ and i is the imaginary number.

It can be shown that (Senjuntichai and Rajapakse, 1995) the general solution of solid and fluid displacements, pore pressure and stresses in the Laplace-Hankel transform space can be expressed in the following matrix form

$$\{\mathbf{v}\} = [\mathbf{R}]\{\mathbf{C}\} \tag{11}$$

$$\{\mathbf{f}\} = [\mathbf{S}]\{\mathbf{C}\} \tag{12}$$

The element v_i (i = 1, 2, 3) of $\{\mathbf{v}\}$ and f_i of $\{\mathbf{f}\}$ are given by

$$v_1(\xi, z, s) = \bar{u}_r, \qquad v_2(\xi, z, s) = \bar{u}_z, \qquad v_3(\xi, z, s) = \bar{p} \tag{13}$$

$$f_1(\xi, z, s) = \bar{\sigma}_{zr}, \qquad f_2(\xi, z, s) = \bar{\sigma}_{zz}, \qquad f_3(\xi, z, s) = \bar{w}_z \tag{14}$$

and the matrices $\mathbf{R}(\xi, z, s)$ and $\mathbf{S}(\xi, z, s)$ are defined in the Appendix. The elements of $\{\mathbf{C}\} = \{A\ B\ C\ D\ E\ F\}$ are the arbitrary functions to be determined by employing appropriate boundary and/or continuity conditions.

3.2 STIFFNESS MATRICES

Consider a multi-layered poroelastic medium with a total of N poroelastic layers overlying a poroelastic half-space with layers and interfaces being numbered as shown in Figure 1. A superscript "n" is used to denote quantities associated with the n^{th} layer (n = 1, 2, . . . , N). For an n^{th} layer, the following relationships can be established by using eqns (11) and (12).

$$\mathbf{U}^{(n)} = \begin{bmatrix} \mathbf{R}^{(n)}(\xi, z_n, s) \\ \cdots\cdots\cdots\cdots \\ \mathbf{R}^{(n)}(\xi, z_{n+1}, s) \end{bmatrix} \mathbf{C}^{(n)} \tag{15}$$

$$\mathbf{F}^{(n)} = \begin{bmatrix} -\mathbf{S}^{(n)}(\xi, z_n, s) \\ \cdots\cdots\cdots\cdots \\ \mathbf{S}^{(n)}(\xi, z_{n+1}, s) \end{bmatrix} \mathbf{C}^{(n)} \tag{16}$$

where

$$\mathbf{U}^{(n)} = \{\mathbf{v}^{(n)}(\xi, z_n, s) \quad \mathbf{v}^{(n)}(\xi, z_{n+1}, s)\} \tag{17}$$

$$\mathbf{F}^{(n)} = \{-\mathbf{f}^{(n)}(\xi, z_n, s) \quad \mathbf{f}^{(n)}(\xi, z_{n+1}, s)\} \tag{18}$$

In eqns (15)–(18), $\mathbf{U}^{(n)}$ denotes a vector of generalized co-ordinates for the n^{th} layer whose elements are related to the Laplace-Hankel transforms of displacements and pore pressure of the top and bottom surfaces of the n^{th} layer. Similarly, $\mathbf{F}^{(n)}$ denotes a generalized force vector whose elements are related to the Laplace-Hankel transforms of tractions and fluid displacements of the top and bottom surfaces of the n^{th} layer. The matrices $\mathbf{R}^{(n)}$ and $\mathbf{S}^{(n)}$ in eqns (15) and (16) are identical to **R** and **S** defined in Appendix except that the material properties of the n^{th} layer are used in the definition and $z = z_n$ and z_{n+1}. The vector $\mathbf{C}^{(n)}$ is the arbitrary coefficient vector corresponding to the n^{th} layer.

The eqn (15) can be inverted to express $\mathbf{C}^{(n)}$ in terms of $\mathbf{U}^{(n)}$ and the substitution in eqn (16) yields

$$\mathbf{F}^{(n)} = \mathbf{K}^{(n)}\mathbf{U}^{(n)}, \quad n = 1, 2, \ldots, N \tag{19}$$

where $\mathbf{K}^{(n)}$ is an exact stiffness matrix in the Laplace-Hankel transform space of the n^{th} layer describing the relationship between the generalized displacement vector $\mathbf{U}^{(n)}$ and the force vector $F^{(n)}$. It is noted that the layer stiffness matrix $K^{(n)}$ is a function of the layer thickness, the layer material properties and the Laplace and Hankel transform parameter s and ξ. For the underlying half-space, the arbitrary function $A^{(n+1)}$, $C^{(n+1)}$ and $E^{(n+1)}$ are set to be zero to gaurantee the regularity of the solutions at infinity.

3.3 GLOBAL STIFFNESS MATRIX

The global stiffness matrix of a multi-layered half-space is assembled by using the layer and half-space stiffness matrices together with the continuity conditions of tractions and fluid flow at layer interfaces. For example, the continuity conditions at the n^{th} interface can be expressed as

$$\mathbf{f}^{(n-1)}(\xi, z_n, s) - \mathbf{f}^{(n)}(\xi, z_n, s) = \mathbf{T}^{(n)} \tag{20}$$

where $\mathbf{f}^{(n)}$ is identical to $\mathbf{f}$ defined in eqn (12) with superscript "n" denoting the layer number and

$$\mathbf{T}^{(n)} = \{ \bar{T}_r^{(n)} \quad \bar{T}_z^{(n)} \quad \frac{\bar{Q}^{(n)}}{s} \} \tag{21}$$

where $\bar{T}_i^{(n)}$ (i = r, z) and $\bar{Q}^{(n)}$ denote the Laplace and Hankel transform of tractions and fluid source which applied at the n^{th} interface, respectively.

The consideration of eqn (20) at each layer interface together with eqn (19) results in the following global equation system

$$\begin{bmatrix} \mathbf{K}^{(1)} & & & \\ & \mathbf{K}^{(2)} & & \\ & & \ddots & \\ & & & \mathbf{K}^{(N)} \quad \mathbf{K}^{(N+1)} \end{bmatrix} \begin{Bmatrix} \mathbf{U}^{(1)} \\ \mathbf{U}^{(2)} \\ \vdots \\ \mathbf{U}^{(N)} \\ \mathbf{U}^{(N+1)} \end{Bmatrix} = \begin{Bmatrix} \mathbf{T}^{(1)} \\ \mathbf{T}^{(2)} \\ \vdots \\ \mathbf{T}^{(N)} \\ \mathbf{T}^{(N+1)} \end{Bmatrix} \tag{22}$$

The solutions of eqn (22) are the influence functions required to establish the flexibility equation for the derivation of the strain energy of a multi-layered poroelastic half-space..

3.4 BOUNDARY CONDITION OF MULTI-LAYERED HALF-SPACE

The plate under this consideration is either fully permeable and impermeable. In order to compute traction and pore pressure which generated between the process of consolidation, eqn (22) is employed together with the following boundary condition

The boundary conditions corresponding to a fully permeable top surface ($z = 0, 0 \le r < \infty$) can be expressed as

$$\sigma_{zi}^{(1)}(r, 0) = 0, \quad i = r, z \tag{23a}$$

$$p^{(1)}(r, 0) = 0 \tag{23b}$$

The continuity conditions at the layer "n" for the case of applied vertical load are given by

$$u_i^{(n-1)}(r, z_n) - u_i^{(n)}(r, z_n) = 0, \quad i = r, z \tag{24a}$$

$$\sigma_{zz}^{(n-1)}(r, z_n) - \sigma_{zz}^{(n)}(r, z_n) = F_z(r) \tag{24b}$$

$$\sigma_{zr}^{(n-1)}(r, z_n) - \sigma_{zr}^{(n)}(r, z_n) = 0 \tag{24c}$$

$$p^{(n-1)}(r, z_n) - p^{(n)}(r, z_n) = 0 \tag{24d}$$

$$w_z^{(n-1)}(r, z_n) - w_z^{(n)}(r, z_n) = 0 \tag{24e}$$

where $F_z(r)$ denotes the intensity of the vertical load applied to a multi-layered half-space.

In order to simulate the pore pressure discontinuity across an impermeable plate, it is necessary to consider the discontinuity of fluid pressure together with vertical stress. Such a problem is described by the following conditions.

$$u_i^{(n-1)}(r, z_n) - u_i^{(n)}(r, z_n) = 0, \quad i = r, z \tag{25a}$$

$$\sigma_{zz}^{(n-1)}(r, z_n) - \sigma_{zz}^{(n)}(r, z_n) = \beta^{(n)}p^{(n)}(r, z_n) - \beta^{(n-1)}p^{(n-1)}(r, z_n) \tag{25b}$$

$$\sigma_{zr}^{(n-1)}(r, z_n) - \sigma_{zr}^{(n)}(r, z_n) = 0 \tag{25c}$$

$$p^{(n)}(r, z_n) - p^{(n-1)}(r, z_n) = P(r) \tag{25d}$$

$$w_z^{(n-1)}(r, z_n) - w_z^{(n)}(r, z_n) = 0 \tag{25e}$$

where P(r) denotes the intensity of fluid pressure discontinuity.

3.5 STRAIN ENERGY OF CIRCULAR PLATE

The deflection of the circular plate in the z-direction denoted by w(r, t) can be represented in the following form:

$$w(r, t) = a_o(t)\, r^2 \ln r + \alpha_1(t) + \sum_{n=2}^{NT} \alpha_n(t)\, r^n, \quad 0 \le r \le 1 \tag{26a}$$

where

$$a_o(t) = P_o H(t)/8\pi D \tag{26b}$$

$$D = E_p h^3/12(1 - \nu_p^2) \tag{26c}$$

In eqn (26a), $\alpha_n(t)$ (n = 1, 2, . . . , NT) denotes a set of generalized co-ordinates, P_o is the magnitude of a concentrated force acting at the center of the plate; H(t) is the Heaviside step

function; h is the thickness of the plate and E_p and ν_p are Young's modulus and Poisson's ratio of the plate material respectively. It may be noted that the term $r^2 \ln r$ in eqn (26a) is included to simulate the singular stress resultants at the plate origin due to the presence of the concentrated force $P_o H(t)$. In the case of a plate subjected only to distributed loading, the first term in eqn (26a) vanishes. By using Laplace transform, eqn (26a) can be expressed in Laplace domain as

$$\overline{w}(r, s) = \bar{a}_o(s)\, r^2 \ln r + \overline{\alpha}_1(s) + \sum_{n=2}^{NT} \overline{\alpha}_n(s)\, r^n, \qquad 0 \le r \le 1 \tag{27}$$

where s denotes the Laplace transform parameter.

The bending moments per unit length denoted by M_r and M_t which act on a circumferential and diametral section of the plate, respectively, can be expressed as

$$M_r = -D\Big[a_o[(1 + 2\ln r)(1 + \nu_p) + 2] + \sum_{n=2}^{NT} n(n - 1 + \nu_p)\, \alpha_n\, r^{n-2}\Big] \tag{28}$$

$$M_t = -D\Big[a_o[(3 + 2\ln r)(1 + \nu_p) - 2] + \sum_{n=2}^{NT} n[(n - 1)\nu_p + 1]\, \alpha_n\, r^{n-2}\Big] \tag{29}$$

and the shear force per unit length, denoted by Q, is given by

$$Q = D\Big[4a_o/r + \sum_{n=3}^{NT} n^2(n - 2)\, \alpha_n\, r^{n-3}\Big] \tag{30}$$

The strain energy, U_p, of a thin elastic plate undergoing axisymmetric flexural deformations is given by (Timoshenko and Woinowsky, 1959)

$$U_p = \pi D \int_0^r \left[\left(\frac{d^2w}{dr^2} + \frac{1}{r}\frac{dw}{dr}\right)^2 - 2(1 - \nu_p)\frac{1}{r}\frac{dw}{dr}\frac{d^2w}{dr^2}\right] r\, dr \tag{31}$$

The substitution of eqn (27) into eqn (31) yields an expression for U_p in terms of generalized co-ordinates $\alpha_2, \alpha_3, \ldots, \alpha_{NT}$. For the purpose of convenient and efficient numerical implementation of the present formulation, the resulting expression for U_p is written in the following matrix form:

$$U_p = (3 + \nu_p)\pi D\, a_o^2 + \langle Q^p \rangle \{\alpha\} + \langle \alpha \rangle [K^p] \{\alpha\} \tag{32}$$

The elements Q_i^p of $\langle Q^p \rangle$ of order NT, and K_{ij}^p of $[K^p]$ of order NT×NT are given by,

$$Q_1^p = 0 \tag{33a}$$

$$Q_i^p = 2\pi D a_o\, [i(3 + \nu_p) - 4] \tag{33b}$$

$$K_{1j}^p = K_{i1}^p = 0 \tag{34a}$$

$$K_{ij}^p = \pi D ij \frac{[ij - 2(i - 1)(1 - \nu_p)]}{(i + j - 2)}, \qquad 2 \le i, j \le NT \tag{34b}$$

3.6 STRAIN ENERGY OF MULTI-LAYERED POROELASTIC MEDIUM

The vertical loading applied to the plate (see Figure 1) is resisted by contact traction, $\overline{T}_z(r, z)$, and pore pressure jumps, $\overline{T}_p(r, z)$, of unknown intensities acting on a circular disc surface S with $0 \le r \le 1$ in the interior of the medium as shown in Figure 2. The contact tractions in radial directions, which are considered to be of secondary importance, are neglected due to the assumption of smooth contact surface.

By using basic relationship from classical elasticity theory (Fung, 1965), the strain energy U_h can be expressed in the form

$$U_h = \frac{1}{2} \int_0^{2\pi} \int_0^1 \overline{T}(r, z)\, w(r)\, r\, dr\, d\theta \tag{35}$$

where $\overline{T}(r, z)$ is the resultant of both T_z and T_p.

The unknown tractions and pore pressure can be expressed in terms of the generalized co-ordinates α_n as

$$T_i = T_{i1}\alpha_1 + \sum_{n=2}^{NT} T_{in}\, \alpha_n + a_o T_i^*, \qquad i = z, p \tag{36}$$

In the present study, the unknown tractions and pore pressure on S are solved by discretizing the surface S into M annular ring elements (Figure 2). It is assumed that T_z and T_p within each ring element are constant and can be evaluated by solving a flexibility equation based on the influence function derived earlier in eqn (22). A coupled flexibility equation can be expressed as

$$[F_{zz}]\, \{T_{zn}\} = \{w_{zn}\}, \qquad n = 1, 2, \ldots, NT \qquad \text{for a permeable plate} \tag{37a}$$

and

$$\begin{bmatrix} [F_{zz}] & [F_{zp}] \\ [F_{pz}] & [F_{pp}] \end{bmatrix} \begin{Bmatrix} \{T_{zn}\} \\ \{T_{pn}\} \end{Bmatrix} = \begin{Bmatrix} \{w_{zn}\} \\ \mathbf{0} \end{Bmatrix}, \qquad n = 1, 2, \ldots, NT \qquad \text{for an impermeable plate} \tag{37b}$$

where F_{ij} denotes the displacement influence function in the i-direction due to a generalized ring load of unit intensity applied in the j-direction. These influence functions are obtained by solving flexibility influence function given in eqn (22).

The elements w_{zni} of $\{w_{zn}\}$ is given by

$$w_{z1i} = 1 \tag{38a}$$

$$w_{zni} = r_i^n, \qquad n = 2, 3, \ldots, NT \tag{38b}$$

The tractions T_z^* and pressure T_p^* acting on the i^{th} ring elements is determined by solving eqn (37) with $w_{zni} = r_i^2 \ln r_i$

The total traction $\overline{T}$ is considered as a resultant of T_z and T_p

$$\overline{T}_{ni} = T_{zni} + \beta T_{pni} \tag{39}$$

From eqns (26) and (39), U_h in eqn (35) can be expressed as

$$U_h = \langle R_z \rangle \{D_z\} \tag{40}$$

The elements of R_{zi} and D_{zi} of $\langle R_z \rangle$ and $\{D_z\}$ are given by

$$R_{zi} = \pi r_i \Delta r_i \left(\sum_{n=1}^{NT} \alpha_n \overline{T}_{ni} + a_o \overline{T}_i^* \right) \tag{41}$$

$$D_{zi} = \alpha_1 + \sum_{n=2}^{NT} \alpha_n r_i^n + a_o r_i^2 \ln r_i \tag{42}$$

In eqn (41)-(42), r_i and Δr_i denote the radial co-ordinate at the centre and width of the i^{th} ring element.

From eqn (40)-(42), the following representation can be established for U_h in terms of $\{\alpha\}$

$$U_h = \langle \alpha \rangle [K^h] \{\alpha\} + \langle Q^h \rangle \{\alpha\} + \pi a_o^2 \sum_{k=1}^{M} \Delta r_k \overline{T}_k^* r_k^3 \ln r_k \tag{43}$$

The elements K_{ij}^h of $[K^h]$, of order NT×NT is given by

$$K_{1j}^h = \pi \sum_{k=1}^{M} r_k \Delta r_k \overline{T}_{jk}, \quad j = 1, 2, \ldots, NT \tag{44a}$$

$$K_{ij}^h = \pi \sum_{k=1}^{M} r_k^{i+1} \Delta r_k \overline{T}_{jk}, \quad j = 1, 2, \ldots, NT;\ i = 2, 3, \ldots, NT \tag{44b}$$

The elements Q_i^h of $\langle Q^h \rangle$ in eqn (43) are given by

$$Q_1^h = \pi a_o \sum_{k=1}^{M} r_k \Delta r_k \left[\overline{T}_k^* + r_k^2 \ln r_k \overline{T}_{1k} \right] \tag{45a}$$

$$Q_i^h = \pi a_o \sum_{k=1}^{M} r_k \Delta r_k \left[r_k^i \overline{T}_k^* + r_k^2 \ln r_k \overline{T}_{ik} \right], \quad i = 2, 3, \ldots, NT \tag{45b}$$

3.7 VARIATIONAL FORMULATION OF INTERACTION PROBLEM

The analysis presented in this thesis is based on the principle of minimum potential energy which state as follows:

> "Of all the displacements which satisfy the boundary conditions of a structural system, those corresponding to stable equilibrium configurations make the total potential energy a relative minimum."

For the system of plate-multi-layered medium as shown in Figure 1, we can express the total potential energy functional, Π, in the form of quadratic function of the generalized co-ordinates α_n (n = 1, 2, . . . , NT) as

$$\begin{aligned}\Pi &= (3+\nu_p)\pi D\, a_o^2 + \pi a_o^2 \sum_{k=1}^{M} \Delta r_k\, \overline{T}_k^{\,*}\, r_k^3 \ln r_k \\ &\quad + \left[\langle Q^p\rangle + \langle Q^h\rangle\right]\{\alpha\} + \langle\alpha\rangle\left[[K^p] + [K^h]\right]\{\alpha\} \\ &\quad - P_o\alpha_1 - 2\pi q_o\left(\frac{\alpha_1}{2} + \sum_{n=2}^{NT} \frac{1}{n+2}\alpha_n\right)\end{aligned} \tag{47}$$

The generalized co-ordinates α_n (n = 1, 2, . . . , NT) are determined by using the principle of minimum potential energy, which requires that

$$\frac{\partial \Pi}{\partial \alpha_n} = 0, \qquad n = 1, 2, \ldots, NT \tag{48}$$

The substitution of eqn (47) into eqn (48) yields the following linear simultaneous equation system:

$$[K^s]\{\alpha\} = \{F^s\} \tag{49}$$

where

$$[K^s] = [K^p] + [K^p]^T + [K^h] + [K^h]^T \tag{50}$$

The elements F_i^s of $\{F^s\}$ are given by

$$F_1^s = P_o + \pi q_o \tag{51a}$$

$$F_i^s = 2\pi q_o/(i+2), \qquad i = 2, 3, \ldots, NT \tag{51b}$$

This system can be solved numerically for a specified geometric configuration and material parameters of the system shown in Figure 1. Thereafter, the plate deflection profile, the plate stress resultants and the net contact stress and pressure acting on the plate can be determined from eqn (26), eqn (27)-(29) and eqn (36), respectively.

CHAPTER IV

NUMERICAL SOLUTIONS

4.1 NUMERICAL SOLUTION SCHEME

Since the present scheme involves the Laplace-Hankel transforms, the time-domain solution is then obtained by numerically evaluating the integrals appearing in eqn (10). The integral with respect to ξ in eqn (10) is evaluated by replacing upper limit with a large number and employing the trapezoidal rule. A review of literature indicates that the Laplace inversion can be carried out very accurately (Piessens, 1975) by using the numerical Laplace inversion method proposed by Stehfest (1970). The formula due to Stehfest is given by

$$f(t) \approx \frac{\ln 2}{t} \sum_{n=1}^{N} c_n \bar{f}\left(n \frac{\ln 2}{t}\right) \tag{52}$$

where $\bar{f}$ denotes the Laplace transform of f(t) and

$$c_n = (-1)^{n+N/2} \sum_{k=[(n+1)/2]}^{\min(n,N/2)} \frac{k^{N/2}(2k)!}{(N/2-k)!k!(k-1)!(n-k)!(2k-n)!} \tag{53}$$

and N is even. It is found that accurate time-domain solutions are obtained from eqn (52) with $N \geq 6$ for poroelasticity problems (Detournay and Cheng, 1988; Rajapakse and Senjuntichai, 1993). It is important to note that the Stehfest method is computationally quite demanding although it is accurate. A more simple and computationally efficient scheme is given by Schapery (1962) which can be expressed as

$$f(t) \approx [s\bar{f}]_{s = 0.5/t} \tag{54}$$

where $\bar{f}$ denotes the Laplace transform of f(t) and s is the Laplace transform parameter.

4.2 COMPARISON WITH EXISTING SOLUTIONS

The convergence and stability of the proposed solution scheme is studied by varying the number of terms NT used in displacement representation given by eqn (26a) and the number of ring elements M used to discretize the circular area S. The following relative rigidity parameter K_r is used in the numerical study,

$$K_r = (1 - \nu_s^2)\frac{E_p}{E_s}\left(\frac{h}{a}\right)^3 \tag{55}$$

where E_s and ν_s are Young's modulus and Poission's ratio of a medium, respectively and h denotes the thickness of a circular plate. Since each layer of multi-layered medium has its own parameter constants, for convenience, all quantities parameters are normalized by corresponding to the top layer of the multi-layered poroelastic half-space.

Table 1. Convergence of solution, W*(0), with NT and M for a centrally loaded plate compare with Rajapakse(1988); H/a = 0.0, ν_s = 0.25, K_r = 0.5, ν_p = 0.3

	W*(0)						
	Present Study						Rajapakse
NT	M = 10	M = 15	M = 20	M = 25	M = 30	M = 35	(1988)
1	0.9420	0.9426	0.9429	0.9431	0.9432	0.9433	0.8478
2	0.8501	0.8506	0.8508	0.8509	0.8510	0.8509	
4	0.8467	0.8473	0.8475	0.8475	0.8476	0.8474	
6	0.8466	0.8472	0.8474	0.8474	0.8475	0.8473	
8	0.8466	0.8472	0.8473	0.8474	0.8474	0.8473	
10	0.8466	0.8471	0.8473	0.8474	0.8474	0.8473	

Table 2. Convergence of solution, M_r*(0.5a), with N and M for a centrally loaded plate compare with Rajapakse(1988); H/a = 0.0, ν_s = 0.25, K_r = 0.5, ν_p = 0.3

	M_r*(0.5a)						
	Present Study						Rajapakse
NT	M = 10	M = 15	M = 20	M = 25	M = 30	M = 35	(1988)
1	0.0225	0.0225	0.0225	0.0225	0.0225	0.0225	0.0116
2	0.0092	0.0093	0.0094	0.0094	0.0094	0.0096	
4	0.0115	0.0115	0.0116	0.0116	0.0116	0.0118	
6	0.0114	0.0115	0.0115	0.0116	0.0116	0.0118	
8	0.0114	0.0114	0.0115	0.0115	0.0116	0.0118	
10	0.0114	0.0114	0.0115	0.0115	0.0116	0.0118	

Table 1 and 2 give the influence of NT and M on the dimensionless central displacement $W^*(0) = aw(0)E_s/P_o$ and moment at r = 0.5a ($M_r^*(0.5a) = M_r(0.5a)/aP_o$), respectively, for a centrally loaded plate resting on the surface of an homogeneous elastic half-space. It appears from Table 1 and 2 that the accurate computation of stress resultants requires NT ≥ 6 terms. For a number of ring elements used to discretize S, the convergence is achieved with M = 20. Similar convergence characteristics are also observed for plates subjected to a uniformly distributed load. Subsequence numerical results are presented for NT = 10 and M = 20.

Table 3 shows a comparison of dimensionless displacements of a rigid permeable plate resting on a free surface of a poroelastic half-space under a concentrated force P_o at the center of the plate. Results give by Yue and Selvadurai (1995) are also presented for comparison. Two numerical Laplace inversion schemes namely Stehfest and Schapery, are used to obtain time-domain solutions. It is evident that the solutions obtained from Stehfest scheme agree more closely with the results presented by Yue and Selvadurai (1995).

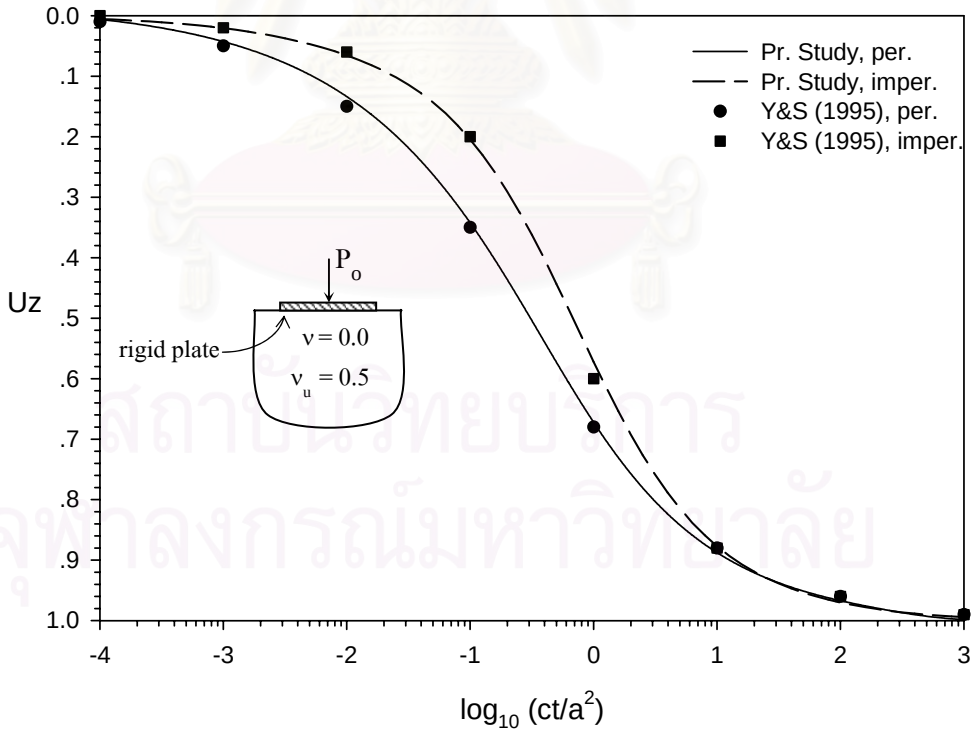

Figure 3. Comparison between degree of consolidation settlement of a centrally loaded rigid plate from present study (H/a = 0.0, ν = 0.0, ν_u = 0.5).

Figure 3 illustrates a comparison between the degree of consolidation displacement from the present study with the one given by Yue and Selvadurai (1995). The degree of consolidation (U_z) is defined as

$$U_z = \frac{w - w_i}{w_f - w_i} \tag{56}$$

where w in eqn (56) denotes the deflection at the centre of the plate and the subscripts i and f denote initial and final solutions. It is evident that the present solutions are consistent with the existing results.

Table 4 shows a comparison of dimensionless radial bending moment $M_r(r)/qa^2$ and tangential bending moment $M_t(r)/qa^2$ along radius of a circular plate with the results presented by Brown (1969) who analyzed a uniformly loaded circular rafts on deep elastic foundations by using power series techniques. Closely agreement between the two solutions is observed for both flexible and relatively rigid plates. In addition, it can be seen that in the case of extremely flexible plate (i.e. $K_r = 0.01$) the maximum bending moment does not occur at the center of the plate.

Figure 4 and 5 show comparison of solution with the results given by Rajapakse and Selvadurai (1991) who considered the interaction between circular footing/anchor plate and non-homogeneous elastic soil. The shear modulus of non-homogeneous soil varies linearly with the depth in the following manner

$$\mu(z) = \mu_o + mz, \quad m > 0 \tag{57}$$

It can be seen from the two figures that the present solutions agree very closely with those presented by Rajapakse and Selvadurai (1991) for both of circular surface footing and anchor plate.

Figures 6(a) and 6(b) show a comparison of axial displacement of the rigid plate with the results from Selvadurai and Yue (1994). The finite layers resting in bonded contact with a rigid impermeable base and the surface of the layer is considered to be either permeable or impermeable. Several combinations of ν and ν_u are used. These results are applicable for $h/a = 1$. The results in those figures show that the difference between the undrained and drained Poissons ratios plays a key role in the consolidation of the plate. The initial response of the non-

dimensional settlements is governed by the undrained Poisson's ratio ν_u. The final response of the non-dimensional settlement is governed by the drained Poisson's ratio ν.

Figures 7(a) and 7(b) illustrate the influence of the hydraulic drainage boundary condition at top and bottom surface. It can be seen from these two figures that the final solution are reached earlier when the bottom surface is permeable.

4.3 NUMERICAL RESULTS AND DISCUSSOION

In this section, three examples of interaction between a plate and a multi-layered poroelastic half-space are presented. The following non-dimensional time factor is employed in the case of multi-layer poroelastic half-space

$$t^* = \frac{c^{(1)}}{a^2} t \tag{58}$$

where the superscript (1) denotes the top most layer of the half-space.

The general behavior of plate-multi-layer poroelastic half-space is illustrated in Problem 1. A layered system consists of two poroelastic layers bonded to an underlying poroelastic half-space, as shown in Figure 8, is considered. Each of layer has thickness equal to radius of a circular plate, "a". The circular plate is resting on the surface of the second layer. The two types of applied loading are considered, i.e., a point load and a uniform distributed load. The numerical results of Problem 1 are shown in Figures 9-22.

Figure 9 shows time histories of dimensionless displacements ($W^* = W(0)a\mu^{(1)}/P_o$) and radial bending moments at $r = 0.01a$ ($M_r^* = M_r(0.01a)/aP_o$) of a centrally loaded plate. For initial time, an impermeable plate has smaller displacement and bending moment than a permeable plate. It is evidence that final solutions of two types of drainage condition are the same. This is due to the fact that for larger time, pore pressure is already dissipated and the consolidation process then finishes. It is also found that the maximum values of displacements and bending moment occur at the end of the consolidation process.

Figure 10 and 11 present dimensionless central displacement histories and dimensionless radial bending moment at $r = 0.01a$, respectively, with various relative rigidity parameter K_r (K_r

= 1, 2, 5, 10, 50, 100, 1000). Again, both of permeable and impermeable plates have different initial displacement and bending moment but have the same final solutions. It is found that the values of K_r have no effect on the rate of consolidation, i.e. all of displacement histories curve almost parallel. But they have a significant influence on the magnitude of the plate displacement. It is also found that magnitude of displacement decreases with increasing the value of K_r and a stiffer plate yields smaller displacement but larger bending moment.

Figure 12 and 13 show variation of displacement profile of flexible plate (K_r = 1) and rigid plate (K_r = 10000), respectively. For both cases, the deflection profile gradually approaches static condition for larger time, i.e. t* = 1000. For a flexible plate, the maximum value of displacement occurs at the center of the plate and the profiles between $0.2a < r < 1$ appear almost straight line. For a rigid plate, the displacement profiles are flat. It is clear that the highest rate of consolidation process occurs for $0.01 < t^* < 1$.

Figure 14 shows variation of final solution (t* = 1000) of displacement and radial bending moment profiles of a centrally loaded plate with relative rigidity K_r (K_r = 1, 2, 5, 10, 50, 1000). It is observed that a flexible plate yields larger deflection and bending moment than a stiff plate.

The effect of type of loading is investigated by changing the applied load from a point load P_o to be a uniform load q_o distributed over an area of plate surface as shown in Figure 15-22. The dimensionless displacement ($W^* = W(r)\mu^{(1)}/aq_o$) and radial bending moment ($M_r^* = M_r(r)/q_o a^2$) are used in the numerical study. Figure 20(b) shows the variation of a bending moment profile with varying relative rigidity parameter K_r. The smooth curves of a bending moment profile is observed with the maximum value occurs at the center of plate. At the edge of the plate, the bending moment converges to zero as in the case of the point load.

Figures 21(a) and 21(b) present the variation of final solution (t* = 1000) of contact stress profiles for both a centrally loaded plate ($q^* = q(r)a^2/P_o$) and a uniformly loaded plate ($q^* = q(r)/q_o$), respectively, with relative rigidity parameter K_r. It can be seen that the magnitude of contact stress adjacent to the center of plate decreases before increasing near the plate edge, when the value of K_r increases. For the case of a point load acting on a flexible plate ($K_r > 2$), the magnitude of contact stress adjacent to center of plate is larger than those near the plate edge. In other cases, the contact stress near the plate edge is much higher than that near the plate center.

Figure 22(a) shows the variation of pore pressure with time of a uniformly loaded plate at position r = 0 and z = a. The interesting phenomenon can be observed that the pore pressure is not decreased immediately but gradually increased for a moment and disappeared rapidly.

Figure 22(b) illustrate the contact stress profiles at bottom surface of the first layer and the top surface of the second layer due to a rigid circular plate subjected a uniform load. It is evidence that the upper interface obtained a small tension and lower interface yield compression.

Figure 23 shows the geometry of problem 2, which is the finite layer problem. The system consists of three poroelastic layers and a circular plate with a point load P_o acting at the center of plate with K_r = 1.0. The thickness of the first and the second layer are equal to the radius of a plate "a". The thickness of the third layer is varied as h_3 = 0.5a, a, 2a, 5a, 10a and infinity for the extreme case of a half-space. The boundary condition of bottom base is specified as an impermeable-rough base ($u_r = u_z = \frac{\partial p}{\partial z} = 0$). The solution of this problem, i.e. central displacement and radial bending moment at r = 0.01a for permeable and impermeable plate, is given in Figures 24 and 25. The trend of the solutions is consistence with the results given before. Both displacement and radial bending moment increase with increasing the thickness of the third layer.

The problem 3, which studies the effect of depth of embedment is shown in Figure 26. This type of problem can be considered as the analysis of a deep foundation. The thickness of second layer is varied as h_2 = 0.5a, a, 2a, 5a, 10a, 50a, 100a, 1000a. The solution of this problem is given in Figure 27-30. The result of this problem shows that deeper footing experiences smaller deflection and bending moment. It is noted that when $h_2 > 50a$ the results (both displacement and bending moment) are almost the same.

Figure 29(b) shows an interesting result that radial bending moment at edge of plate converge to zero although the depth of embedment is equal to 1000a. From this result it can be concluded that the depth of embedment does not effect the plate edge boundary condition.

Figure 30 presents the effect of relative rigidity parameter K_r to the displacement and radial bending moment. It is evidence that when $K_r > 1000$, both the plate deflection and bending moment are constant. It can then be concluded that rigid plate behavior can be obtained by setting $K_r > 1000$.

CHAPTER V

CONCLUSIONS

The quasi-statics response of an axisymmetric-loaded circular plate buried in a multi-layered poroelastic half-space is analyzed by using a variational method of analysis. The assumed deflected shape is indeterminated with a set of arbitrary constants. The total potential energy functional consists of the strain energy of multi-layered media, the strain energy of the circular plate and the potential energy of the applied loads. The unknown constants are obtained from the linearly independent algebraic equations generated from the minimization of the total potential energy functional. The accuracy of the present scheme is confirmed by comparing with the existing results.

Numerical solutions presented in the chapter IV demonstrate the applicability of the present solution scheme. Selected numerical results for different layered systems indicate that the behavior of the plate is governed by various parameters. The influence of these parameters on the plate and a multi-layered poroelastic half-space system can be summarized as follows:

1.) The deflection of the circular plate decreases rapidly with increasing values of the relative rigidity parameter K_r of the plate, and a plate with $K_r \geq 1000$ can be considered as a rigid plate.

2.) The final solution is obtained when $t^* > 100$.

3.) The hydraulic boundary conditions at the plate-half-space interface, i.e. permeable and impermeable plate surface, have significant influence on the consolidation process. However, the final solution of both cases are equal.

The present method can also be extended to analyze the various types of interaction problems, for example, the problem of arbitrary axisymmetric loads, the problem of a ring plate and the problem of multiple anchor plates, etc.

Table 3. Comparison of dimensionless displacements, $a\mu w/P_o$, of a rigid circular plate.

ct/a^2	$\nu = 0.0$			$\nu = 0.1$			$\nu = 0.2$		
	Current Study		Yue & Selvadurai (1995)	Current Study		Yue & Selvadurai (1995)	Current Study		Yue & Selvadurai (1995)
	Schapery	Stehfest		Schapery	Stehfest		Schapery	Stehfest	
0.04	0.162	0.157	0.156	0.157	0.153	0.152	0.151	0.148	0.147
0.16	0.183	0.178	0.177	0.173	0.170	0.168	0.163	0.160	0.159
0.36	0.196	0.193	0.191	0.184	0.181	0.180	0.171	0.169	0.168
0.64	0.205	0.203	0.202	0.191	0.190	0.188	0.176	0.175	0.174
1.00	0.212	0.211	0.210	0.196	0.196	0.194	0.180	0.180	0.178
1.44	0.217	0.217	0.215	0.200	0.200	0.199	0.183	0.183	0.181
1.96	0.221	0.221	0.220	0.203	0.204	0.202	0.185	0.185	0.184

ct/a^2	$\nu = 0.3$			$\nu = 0.4$		
	Current Study		Yue & Selvadurai (1995)	Current Study		Yue & Selvadurai (1995)
	Schapery	Stehfest		Schapery	Stehfest	
0.04	0.144	0.142	0.141	0.136	0.134	0.134
0.16	0.152	0.150	0.149	0.140	0.139	0.138
0.36	0.157	0.155	0.155	0.142	0.142	0.141
0.64	0.161	0.160	0.159	0.144	0.143	0.143
1.00	0.163	0.163	0.162	0.145	0.145	0.144
1.44	0.165	0.165	0.164	0.146	0.146	0.145
1.96	0.166	0.166	0.165	0.147	0.146	0.145

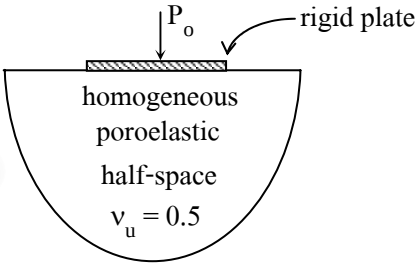

Table 4(a). Comparison of dimensionless radial bending moment ($M_r^* = M_r(r)/q_o a^2$).

r/a	K_r = 0.01		K_r = 0.1		K_r = 1		K_r = 10	
	Present study	Brown (1969)	Present study	Brown (1969)	Present study	Brown (1969)	Present study	Brown (1969)
0.0	0.0012	0.0012	0.0145	0.0146	0.0554	0.0567	0.0726	0.0747
0.1	0.0012	0.0012	0.0145	0.0146	0.0548	0.0561	0.0717	0.0737
0.2	0.0013	0.0013	0.0145	0.0146	0.0528	0.0541	0.0688	0.0708
0.3	0.0014	0.0014	0.0143	0.0145	0.0495	0.0508	0.0640	0.0659
0.4	0.0016	0.0016	0.0140	0.0142	0.0448	0.0461	0.0574	0.0593
0.5	0.0018	0.0018	0.0133	0.0136	0.0389	0.0401	0.0492	0.0509
0.6	0.0021	0.0021	0.0121	0.0125	0.0316	0.0329	0.0394	0.0411
0.7	0.0023	0.0024	0.0101	0.0106	0.0234	0.0246	0.0286	0.0301
0.8	0.0023	0.0024	0.0071	0.0076	0.0143	0.0154	0.0171	0.0184
0.9	0.0015	0.0017	0.0032	0.0037	0.0055	0.0063	0.0063	0.0072
1.0	0.0000	0	-0.0001	0	-0.0001	0	-0.0001	0

Table 4(b). Comparison of dimensionless tangential bending moment ($M_t^* = M_t(r)/q_o a^2$)

r/a	K_r = 0.01		K_r = 0.1		K_r = 1		K_r = 10	
	Present study	Brown (1969)	Present study	Brown (1969)	Present study	Brown (1969)	Present study	Brown (1969)
0.0	0.0012	0.0012	0.0145	0.0146	0.0554	0.0567	0.0726	0.0747
0.1	0.0012	0.0012	0.0145	0.0146	0.0551	0.0564	0.0721	0.0741
0.2	0.0012	0.0012	0.0145	0.0146	0.0539	0.0552	0.0705	0.0724
0.3	0.0013	0.0013	0.0144	0.0146	0.0520	0.0533	0.0677	0.0696
0.4	0.0014	0.0014	0.0143	0.0144	0.0493	0.0506	0.0639	0.0658
0.5	0.0015	0.0015	0.0139	0.0142	0.0459	0.0472	0.0590	0.0609
0.6	0.0017	0.0017	0.0134	0.0136	0.0417	0.0430	0.0533	0.0551
0.7	0.0019	0.0019	0.0124	0.0127	0.0369	0.0381	0.0469	0.0486
0.8	0.0019	0.0020	0.0110	0.0114	0.0315	0.0327	0.0399	0.0415
0.9	0.0017	0.0018	0.0091	0.0095	0.0260	0.0271	0.0328	0.0343
1.0	0.0011	0.0012	0.0072	0.0074	0.0214	0.0222	0.0271	0.0283

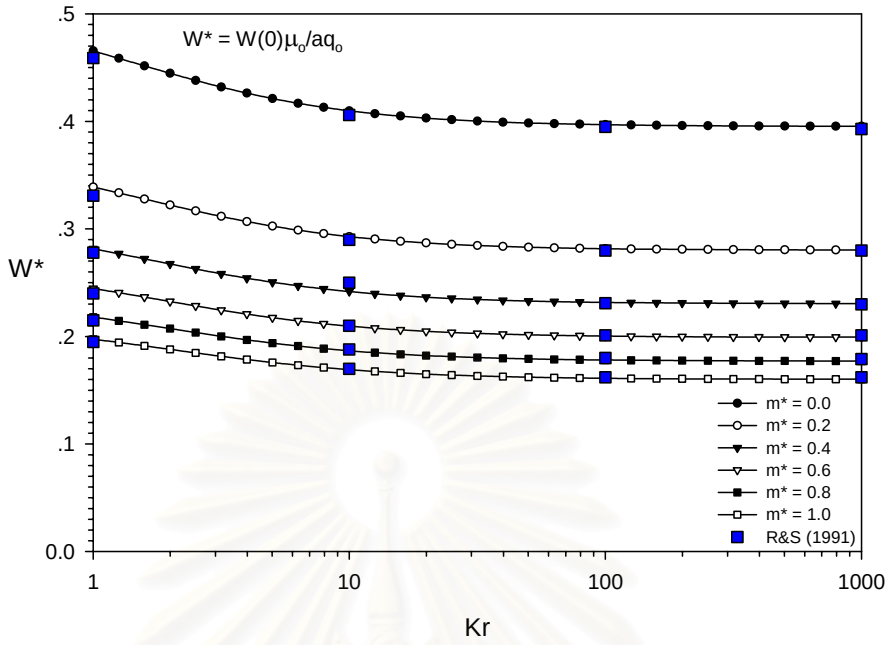

Figure 4. Comparison of variation of normalized central deflection of a uniformly loaded plate with relative rigidity K_r and degree of non-homogeneity, m*, (from present study with results from Rajapakse and Selvadurai, 1991).

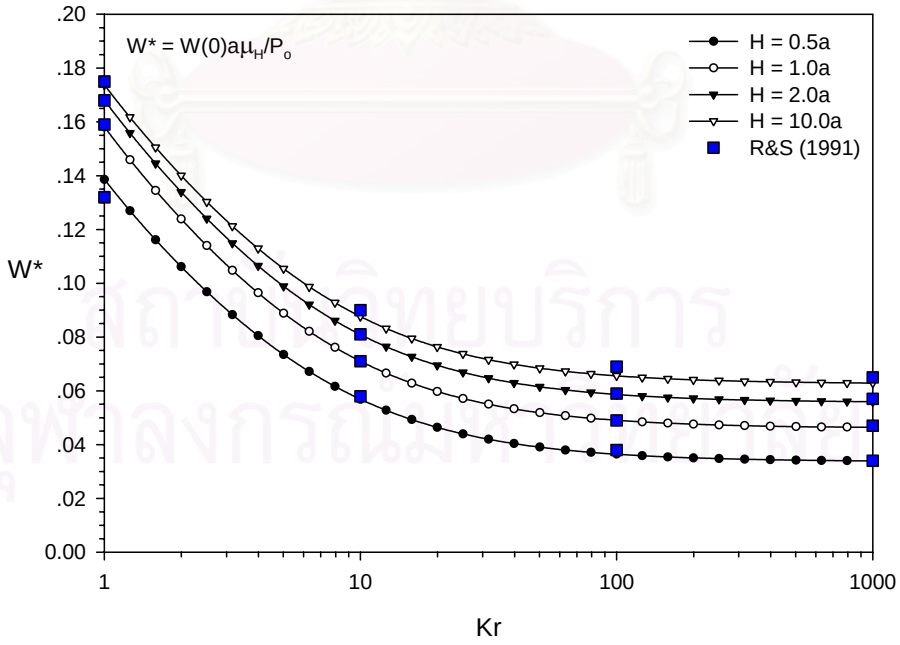

Figure 5. Comparison of variation of normalized central deflection of anchor plates with relative rigidity K_r and depth of embedment for a soil with $\mu_o = 0$, (from present study with results from Rajapakse and Selvadurai, 1991).

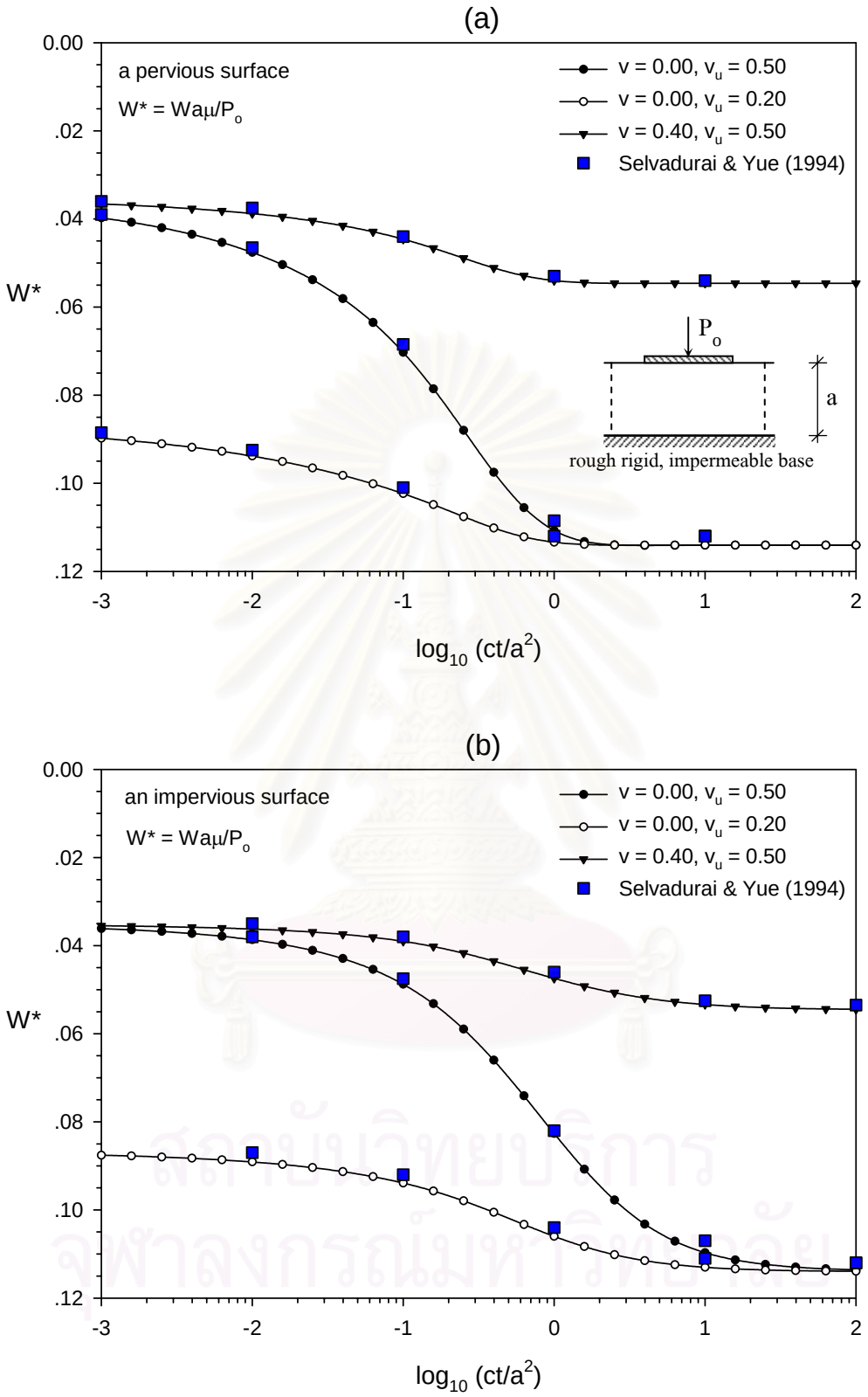

Figure 6. Comparison of axial displacement of the rigid plate.

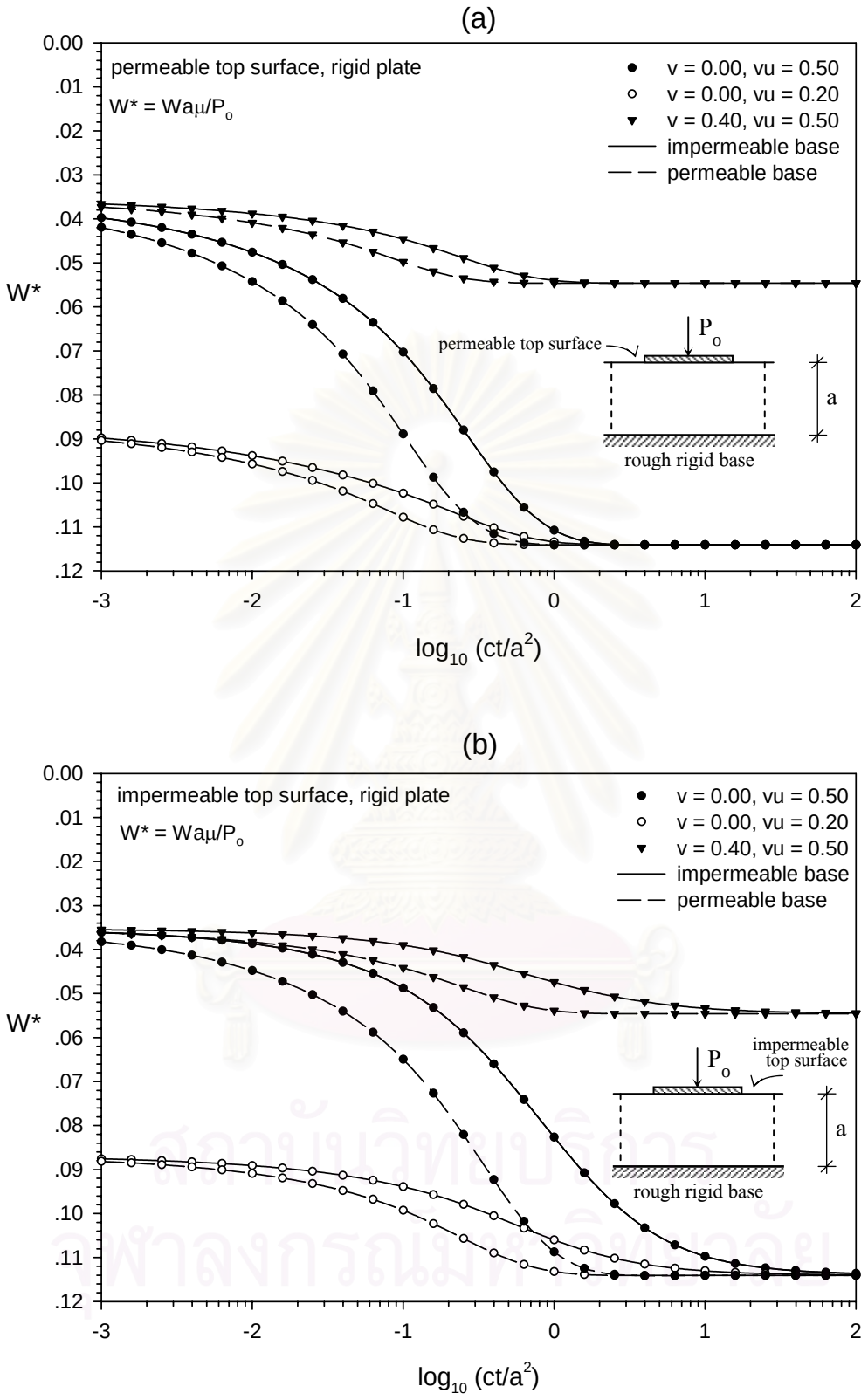

Figure 7. Effect of Poisson's ratios and surface drainage on the consolidation induced axial displacement of the rigid punch.

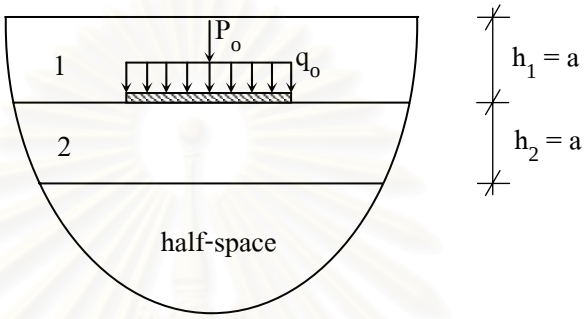

	B	ν	ν_u	$\mu^{(i)}/\mu^{(1)}$	$\kappa^{(i)}/\kappa^{(1)}$
1st layer	1.0	0.25	0.50	1	1
2nd layer	0.8	0.20	0.35	2	10
half-space	0.6	0.15	0.30	3	0.5

Figure 8. Geometry of problem 1.

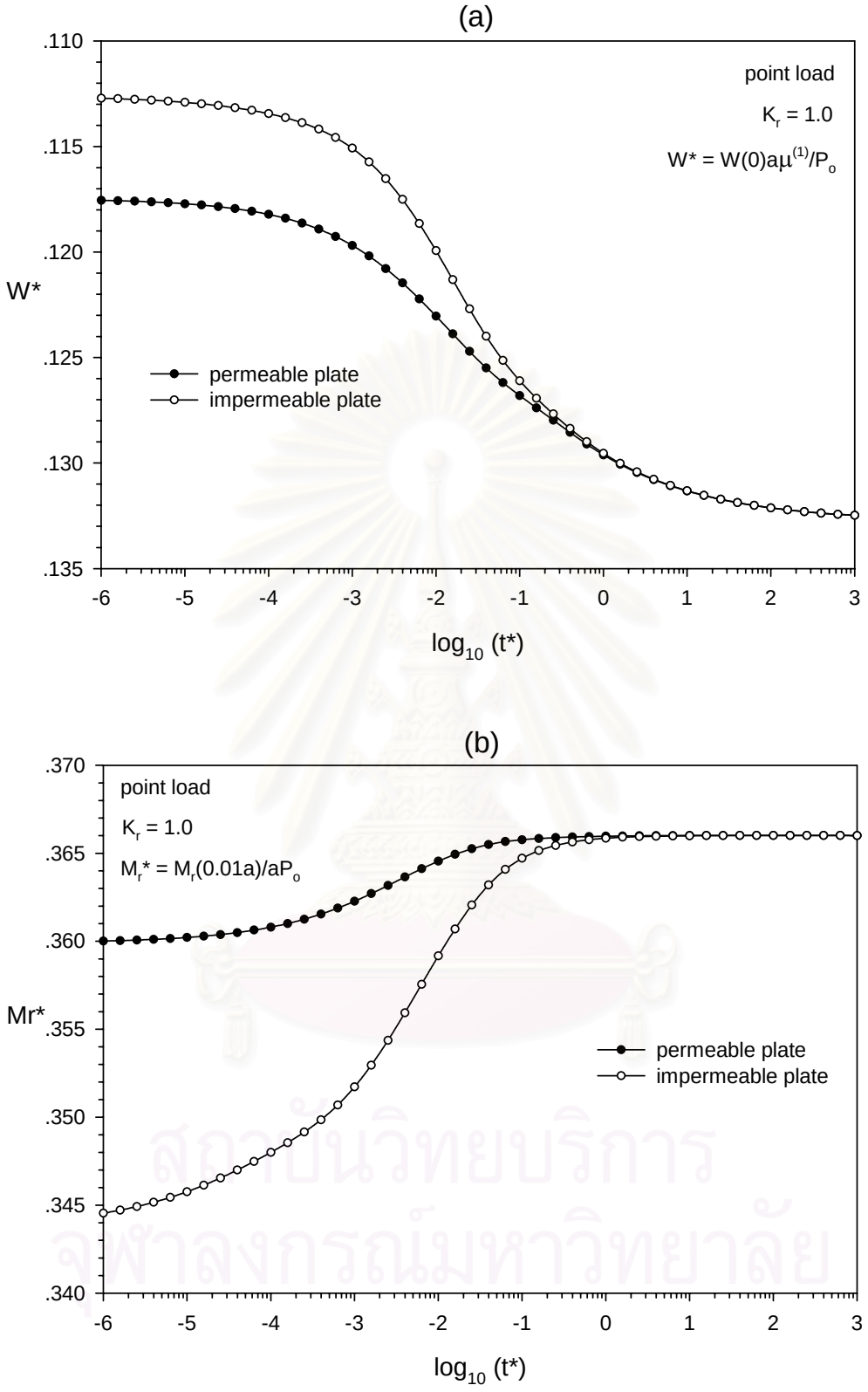

Figure 9. Variation of (a) dimensionless central displacement W*(0) and (b) radial bending moment M_r*(0.01a) of a centrally loaded plate with time and drainage boundary condition.

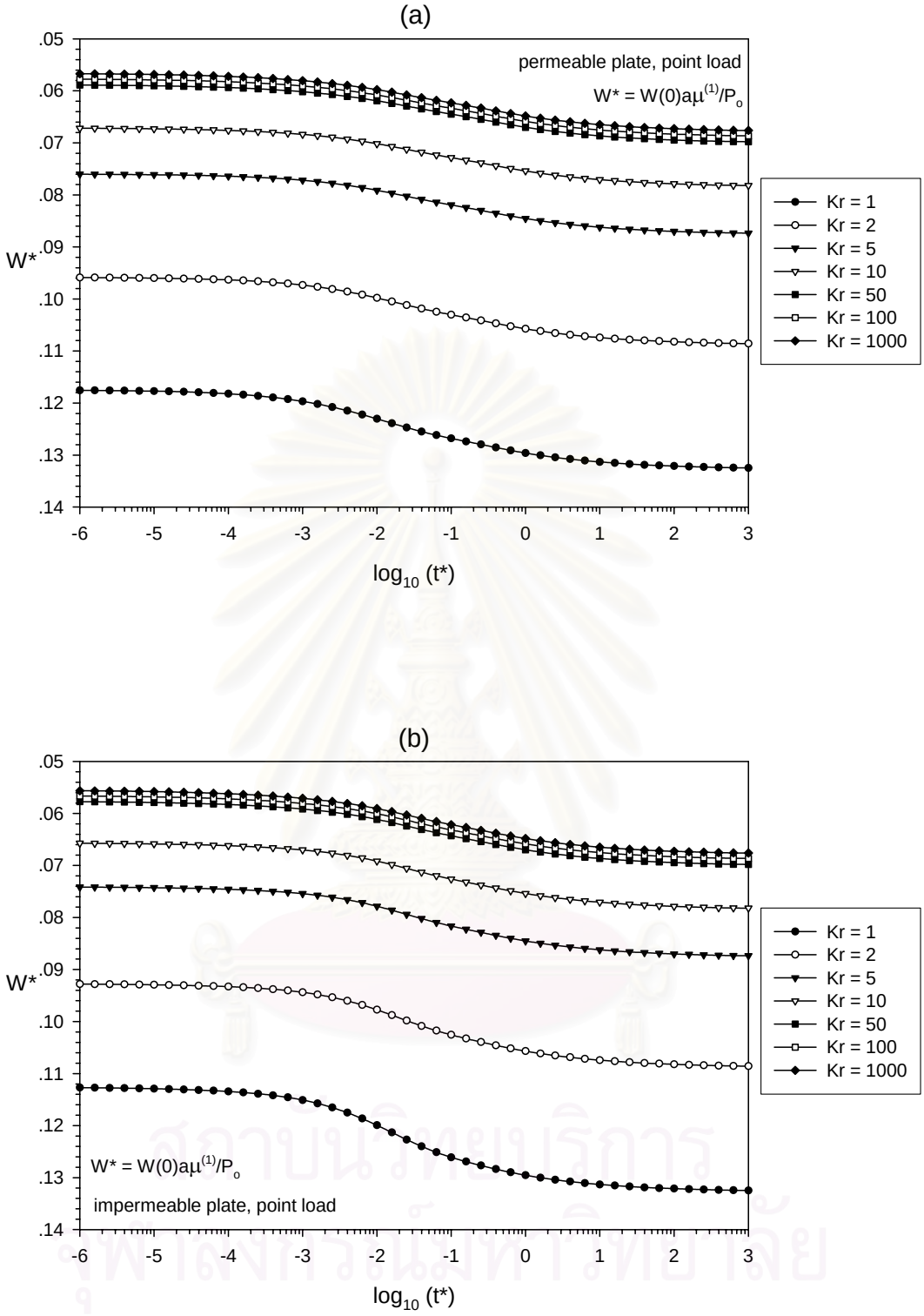

Figure 10. Variation of dimensionless central displacement W*(0) of a centrally loaded plate with time and relative rigidity parameter K_r.

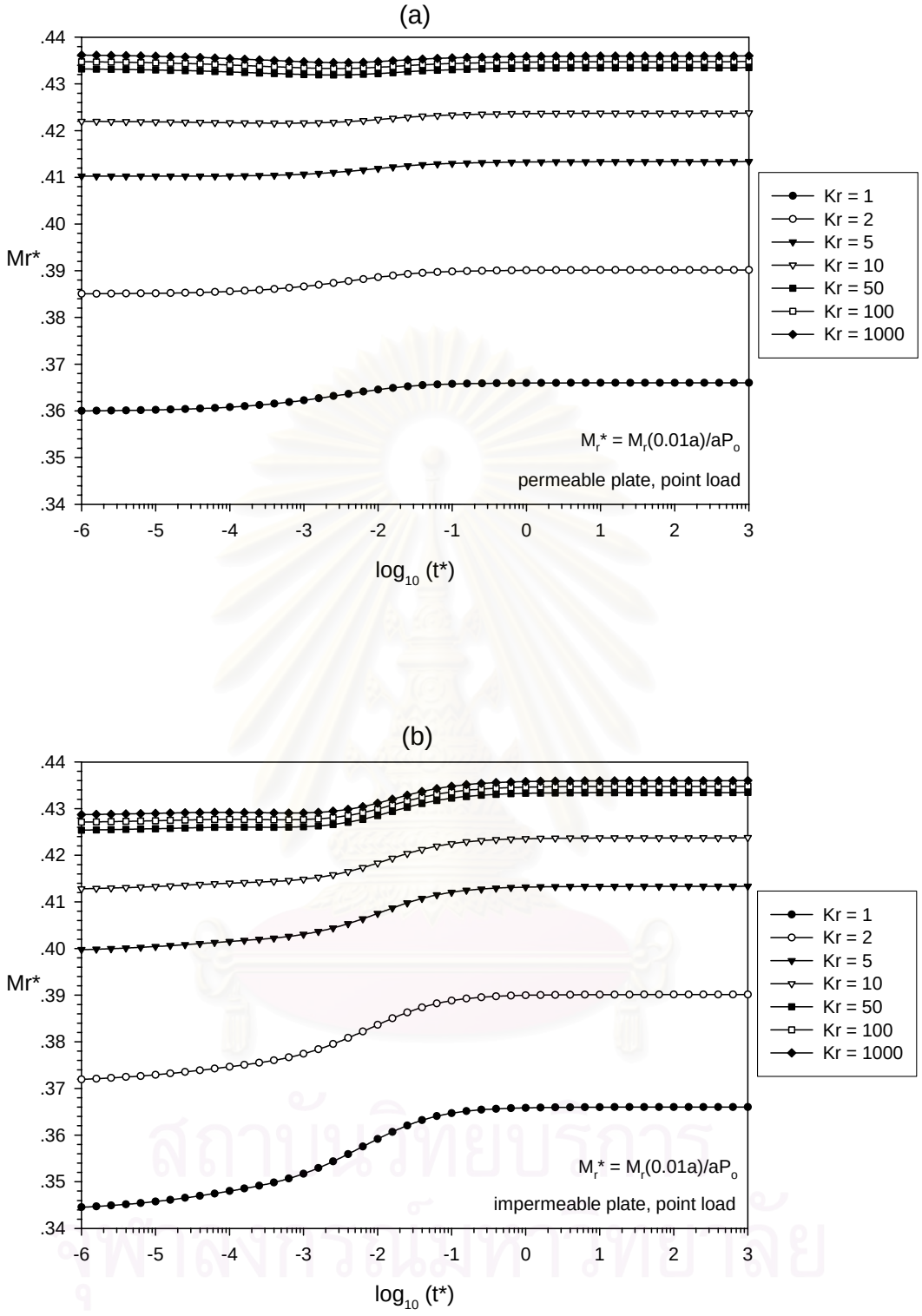

Figure 11. Variation of radial bending moment M_r*(0.01a) of a centrally loaded plate with time and relative rigidity paraemter K_r.

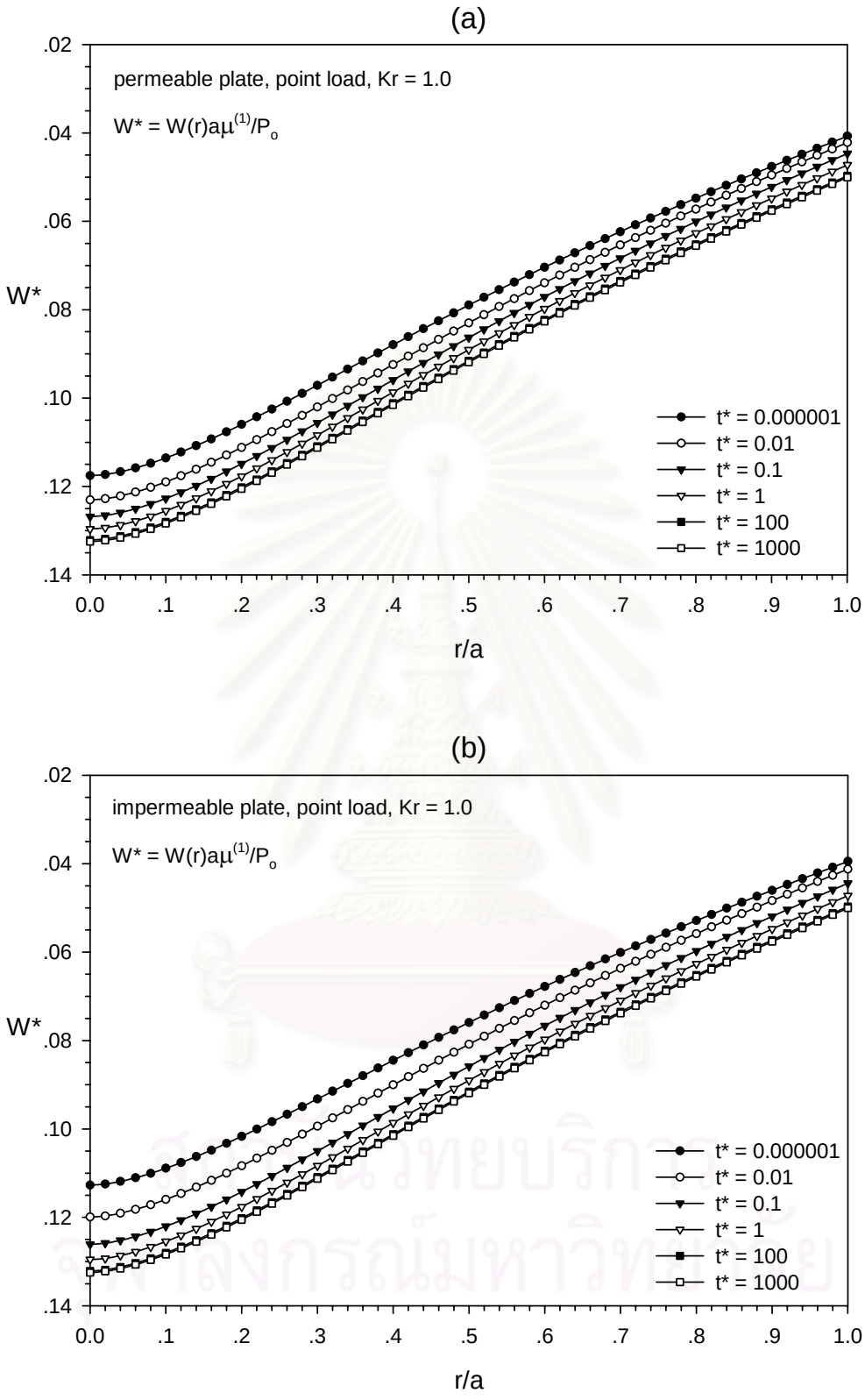

Figure 12. Variation of displacement profile of a centrally loaded plate (K_r = 1.0) with times.

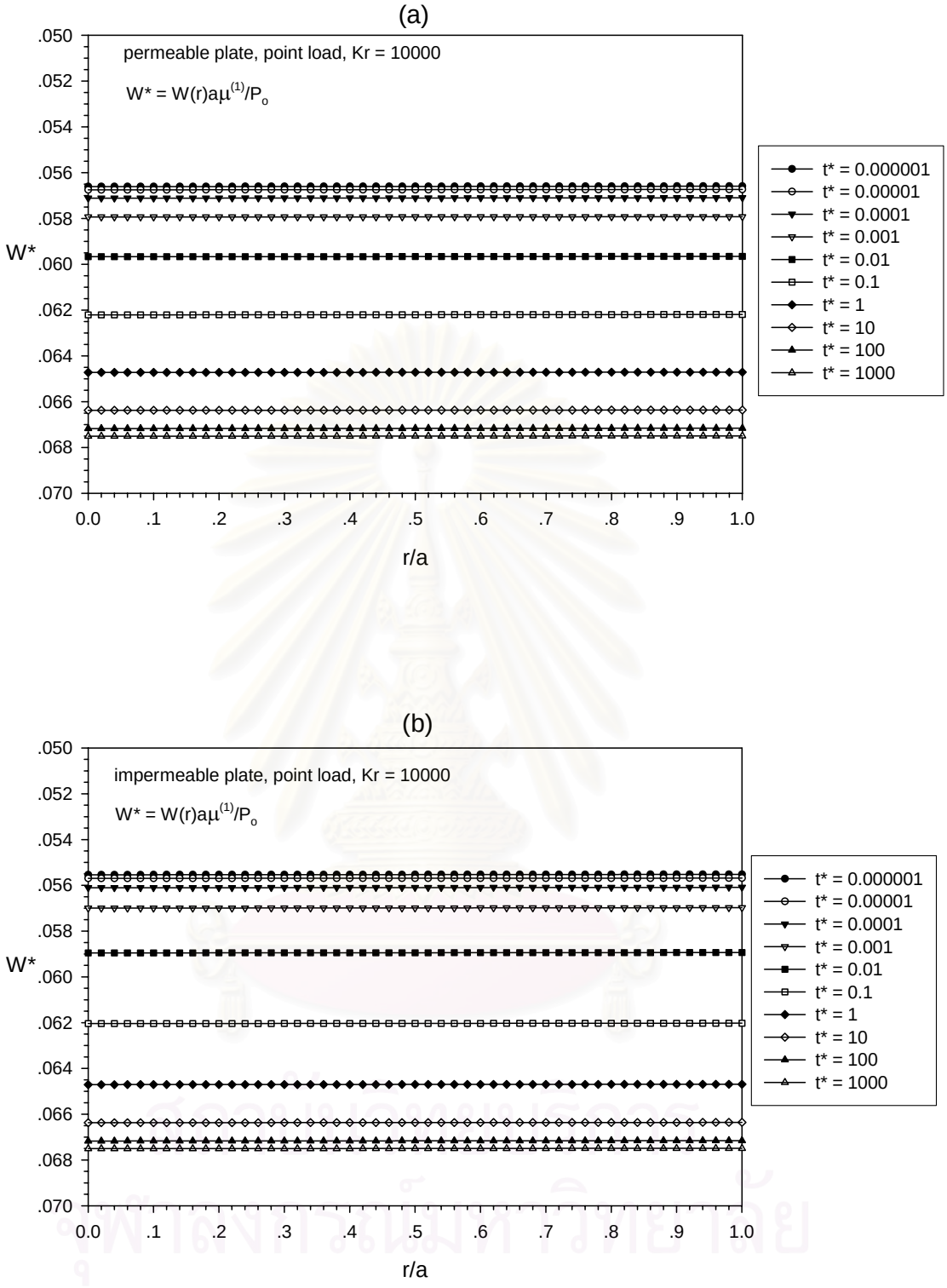

Figure 13. Variation of displacement profile of a centrally loaded rigid plate (K_r = 10000) with times.

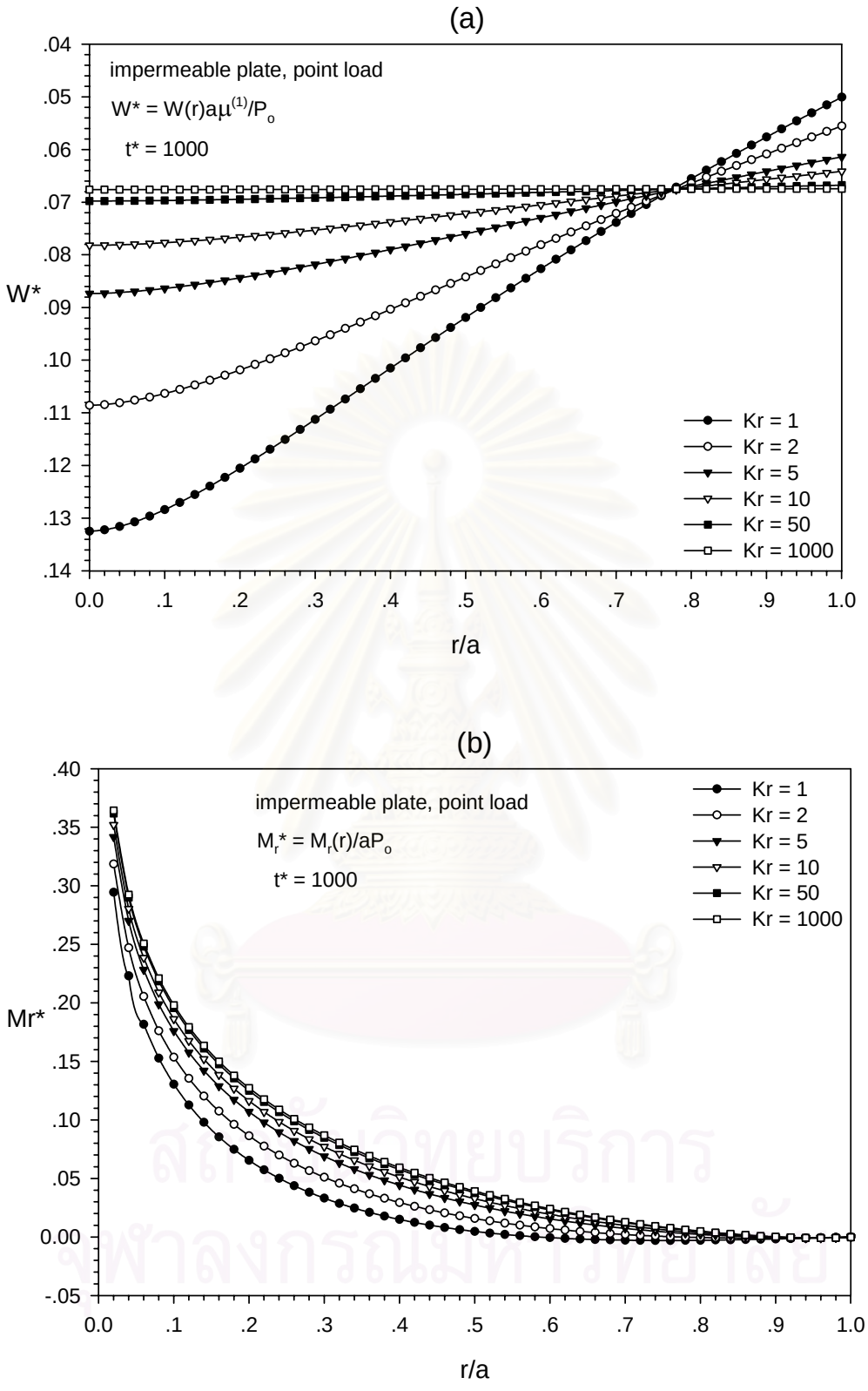

Figure 14. Variation of (a) displacement profile and (b) radial bending moment profile of a centrally loaded plate with relative rigidity K_r.

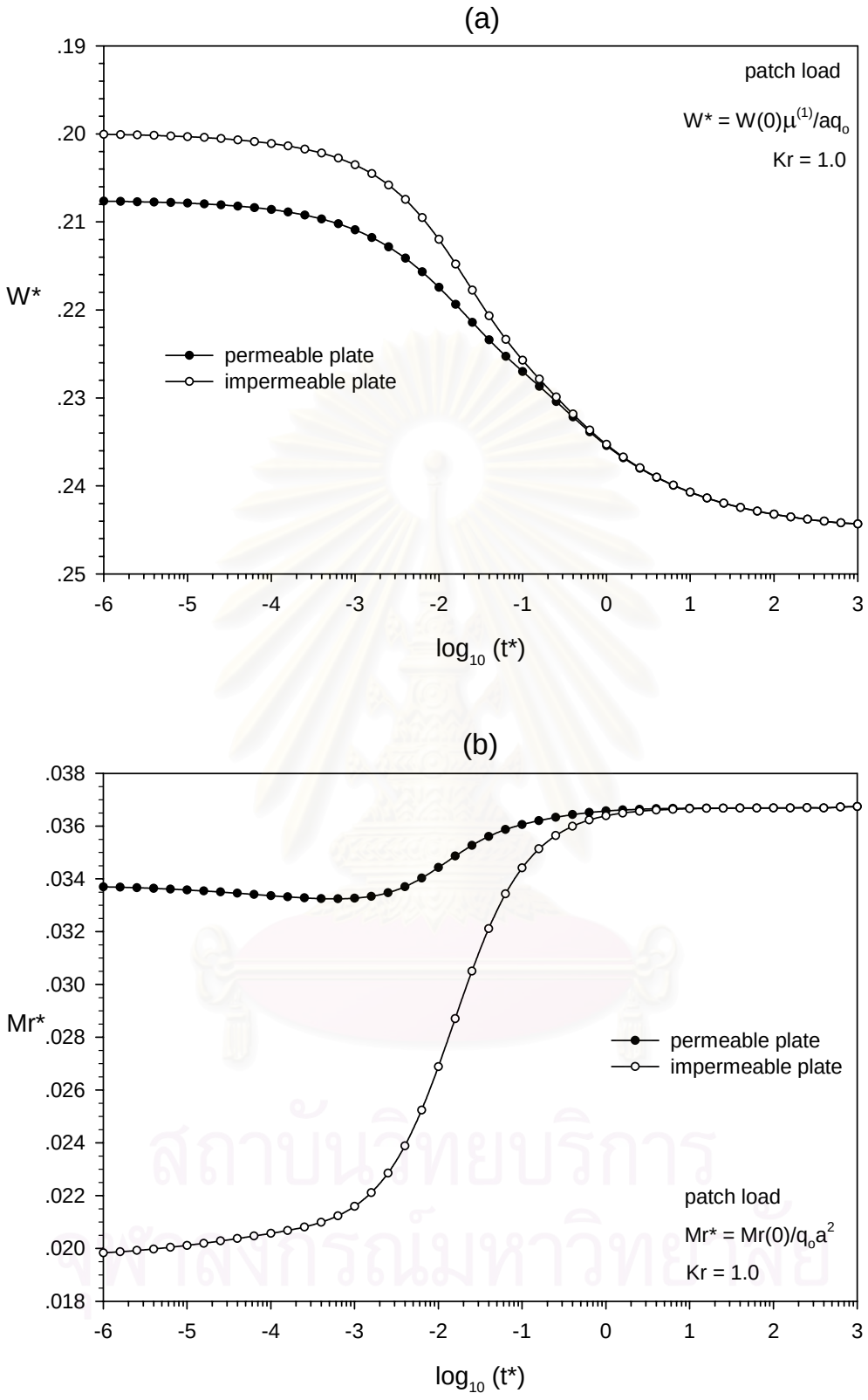

Figure 15. Variation of (a) dimensionless central displacement W*(0) and (b) radial bending moment M_r*(0) of a uniformly loaded plate with time and drainage boundary condition.

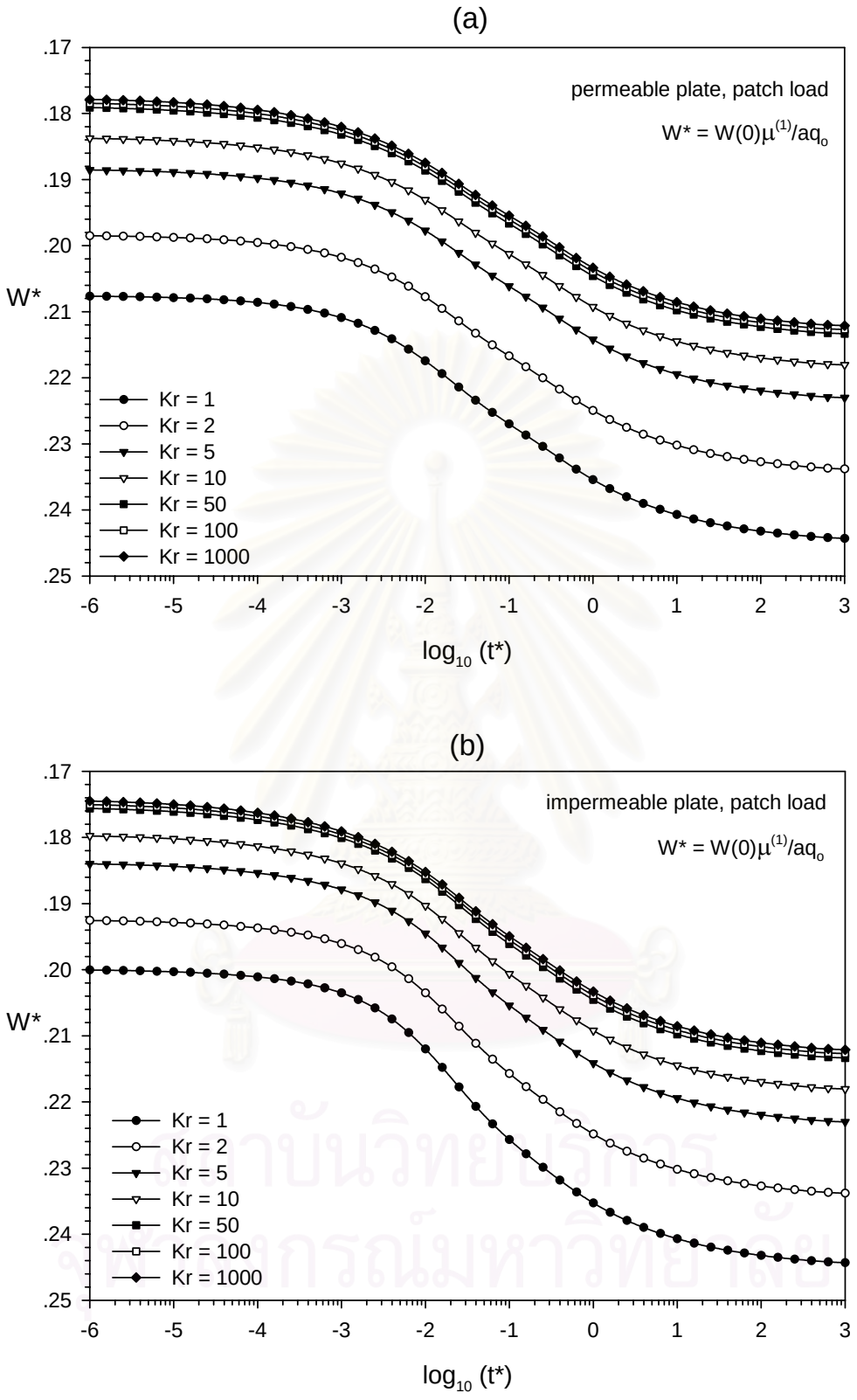

Figure 16. Variation of dimensionless central displacement W*(0) of a uniformly loaded plate with time and relative rigidity parameter K_r.

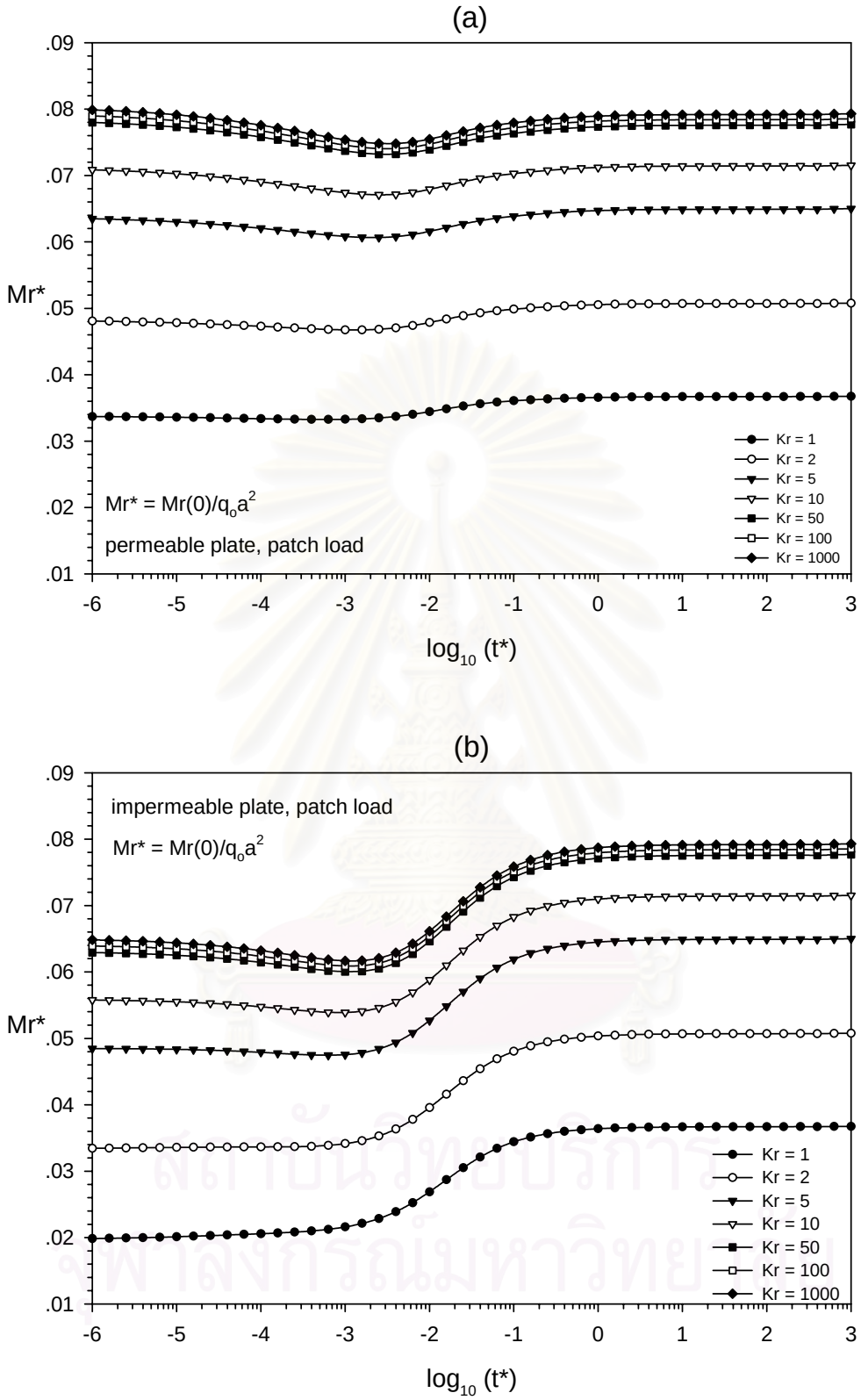

Figure 17. Variation of dimensionless radial bending moment $M_r^*(0)$ of a uniformly loaded plate with time and relative rigidity parameter K_r.

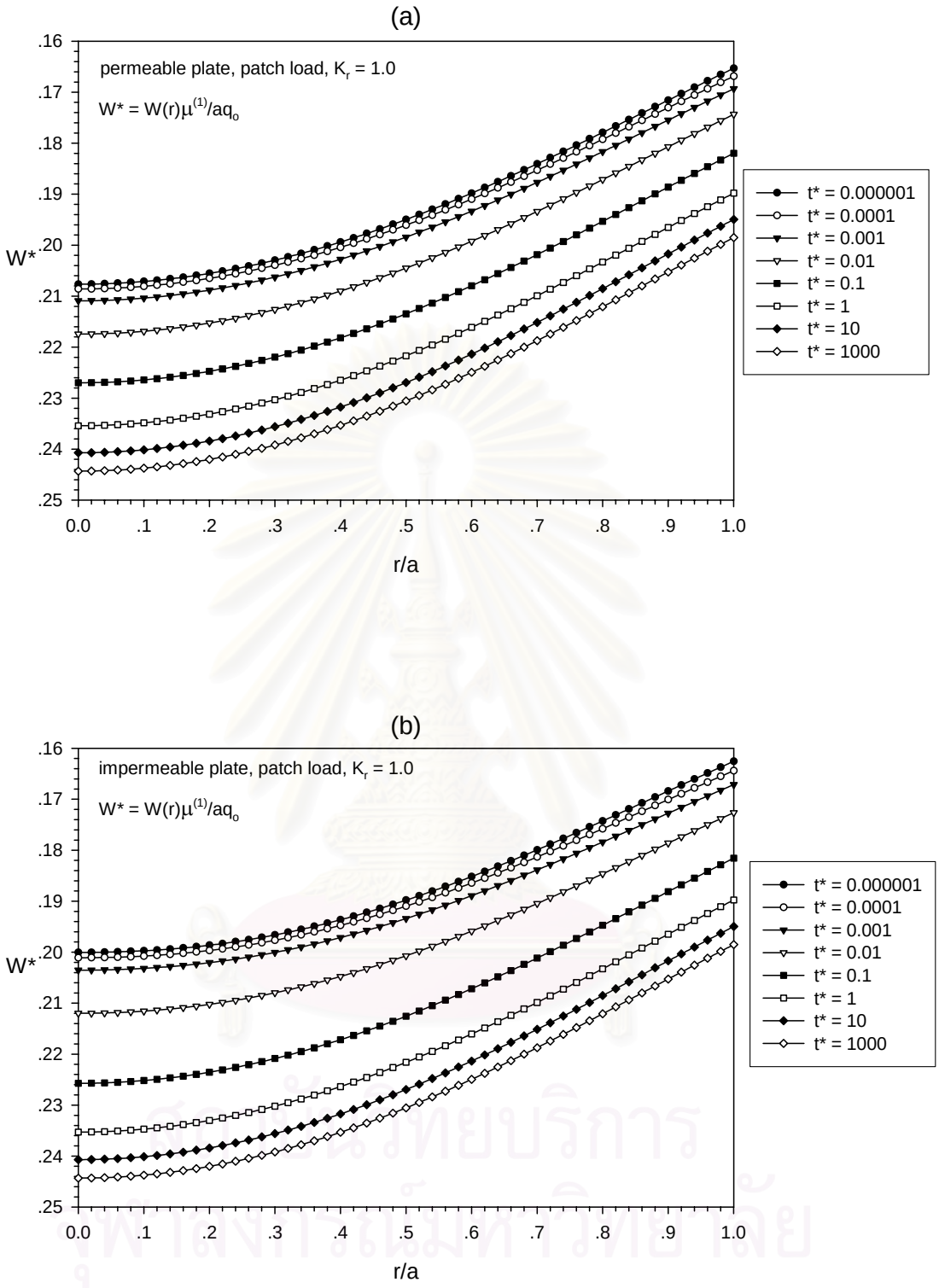

Figure 18. Variation of displacement profile of a uniformly loaded plate (K_r = 1.0) with times.

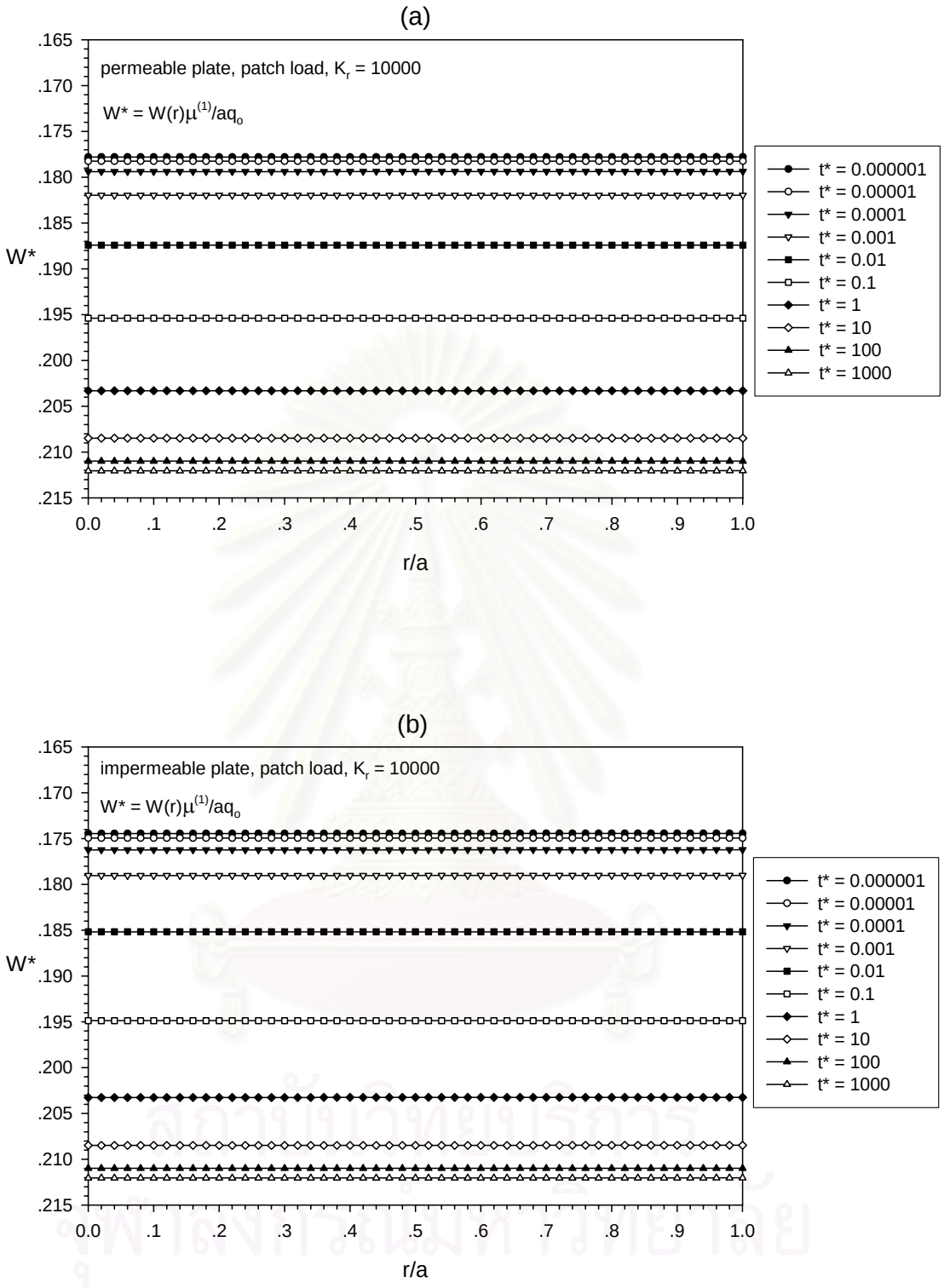

Figure 19. Variation of displacement profile of a uniformly loaded rigid plate (K_r = 10000) with times.

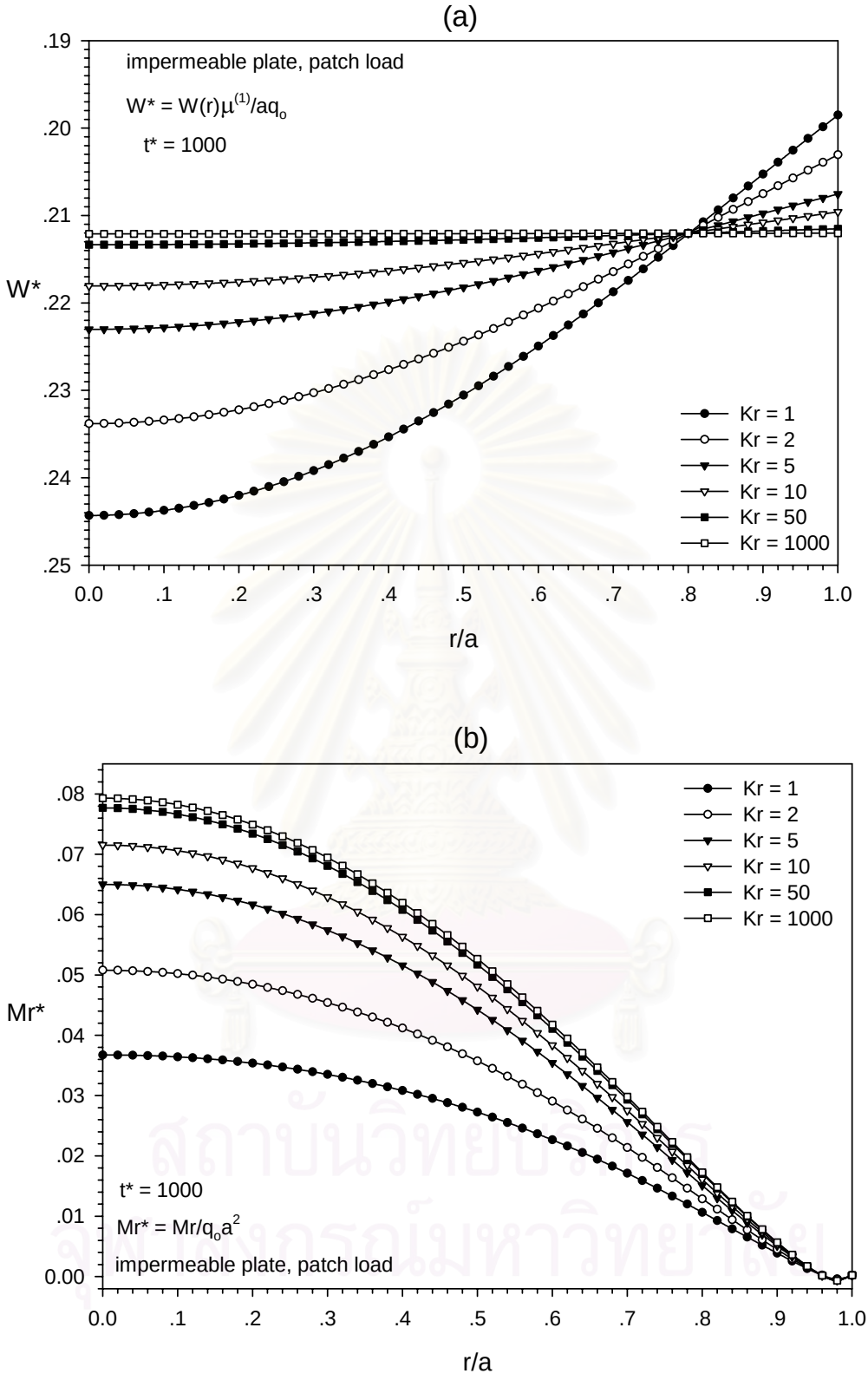

Figure 20. Variation of (a) displacement profile and (b) radial bending moment profile of a uniformly loaded plate with relative rigidity K_r.

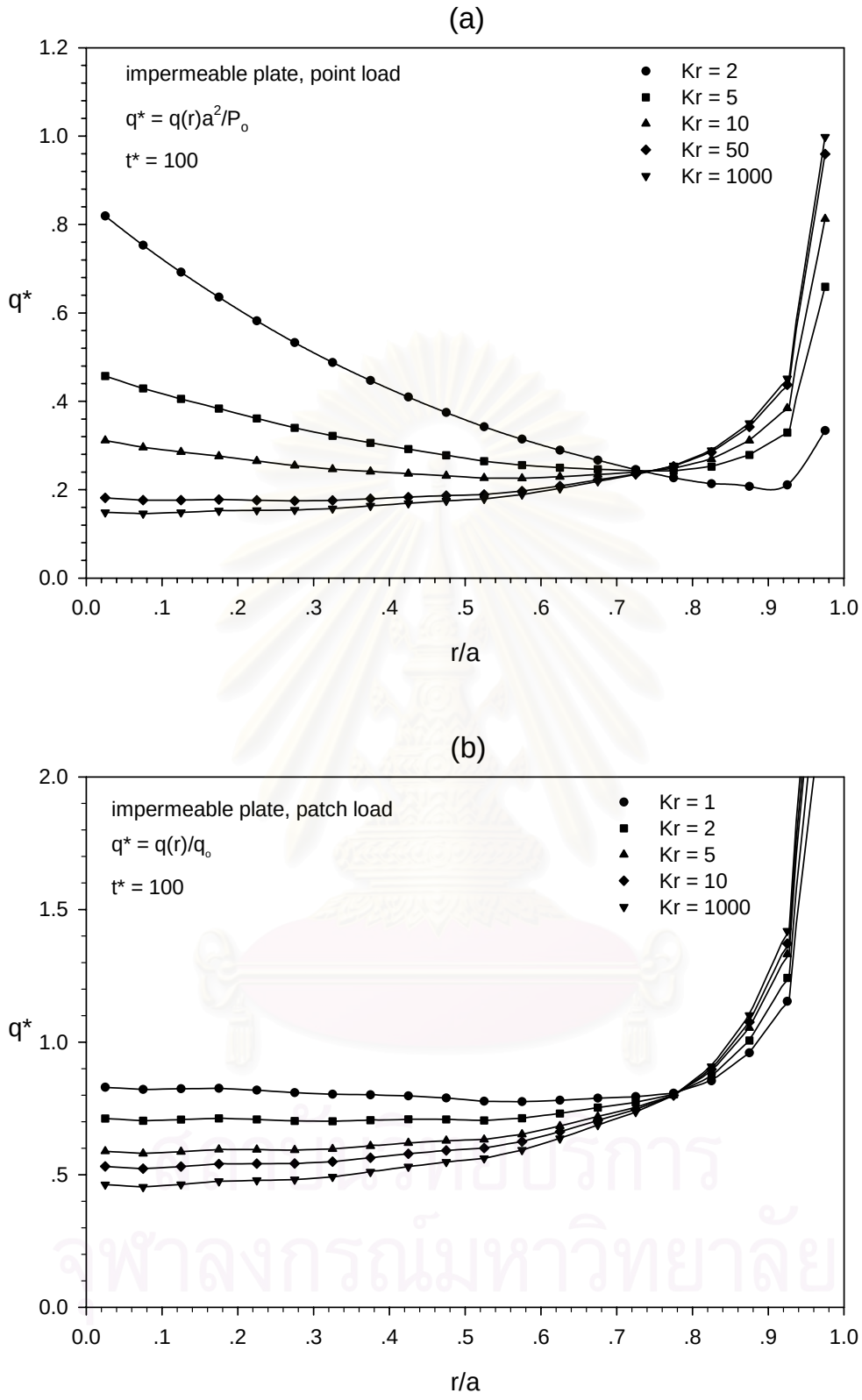

Figure 21. Variation of contact stress profile of (a) a centrally loaded plate and (b) a uniformly loaded plate with relative rigidity K_r.

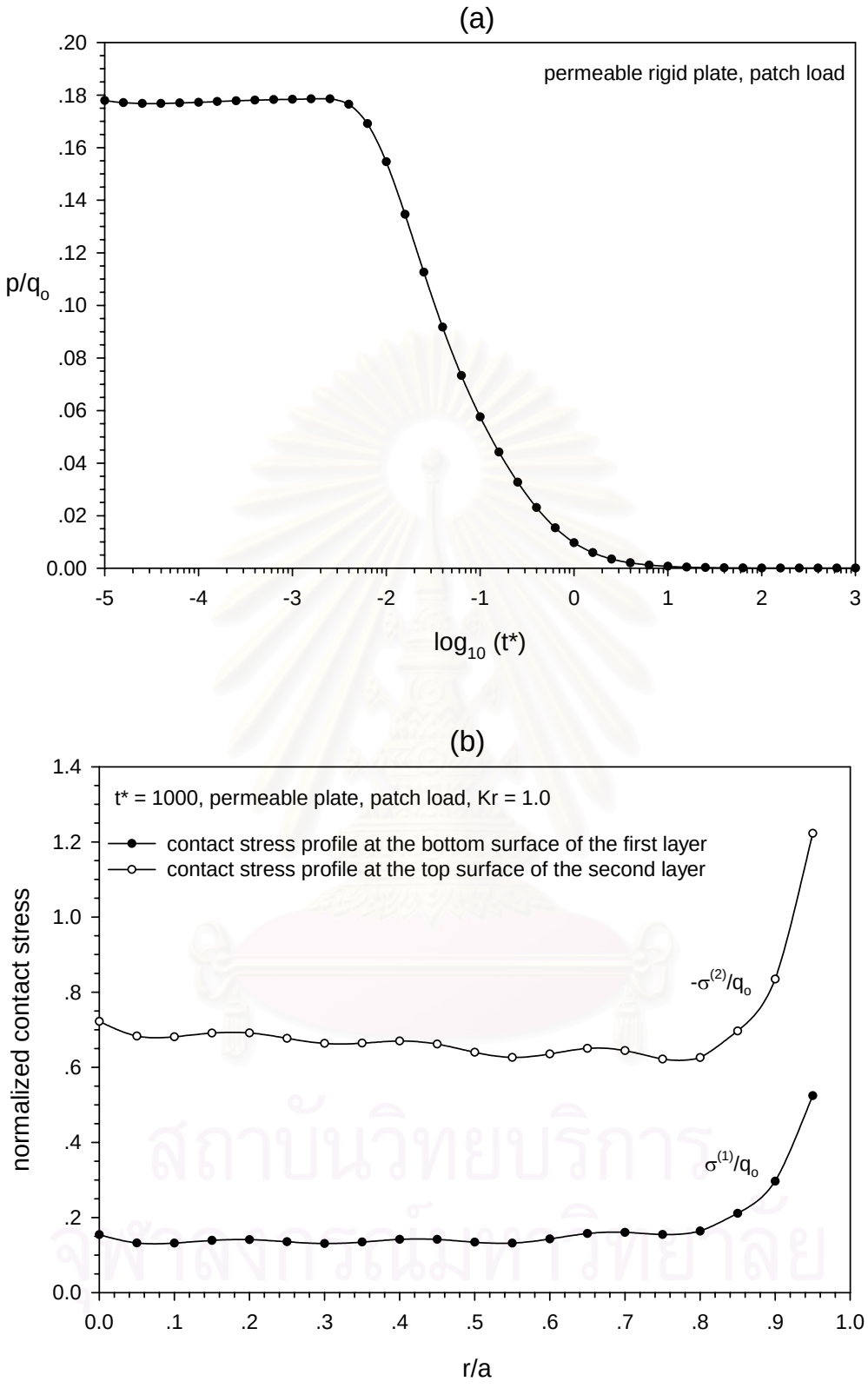

Figure 22. (a) Pore pressure history beneath the plate (z = a, r = 0). (b) Final solution of the contact stress profiles at the bottom surface of the first layer and the top surface of the second layer due to a circular plate subjected a uniform load.

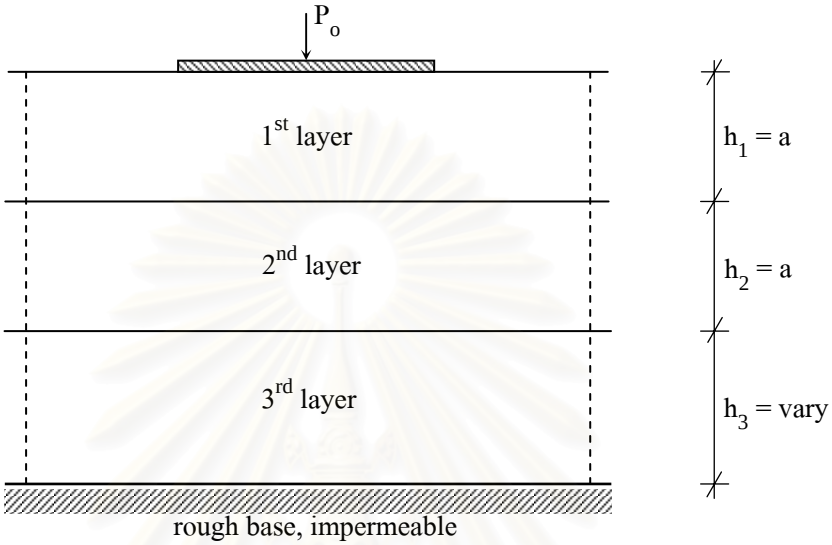

	B	ν	ν_u	$\mu^{(i)}/\mu^{(1)}$	$\kappa^{(i)}/\kappa^{(1)}$
1st layer	1.0	0.25	0.50	1	1
2nd layer	0.8	0.20	0.35	2	0.1
3rd layer	0.6	0.15	0.30	10	0.01

h_3 = 0.5a, a, 2a, 5a, 10a, infinity (half-space)

boundary condition for impermeable rough base $u_r = u_z = 0$ and $\frac{\partial p}{\partial z} = 0$ at bottom base

Figure 23. Geometry of problem 2.

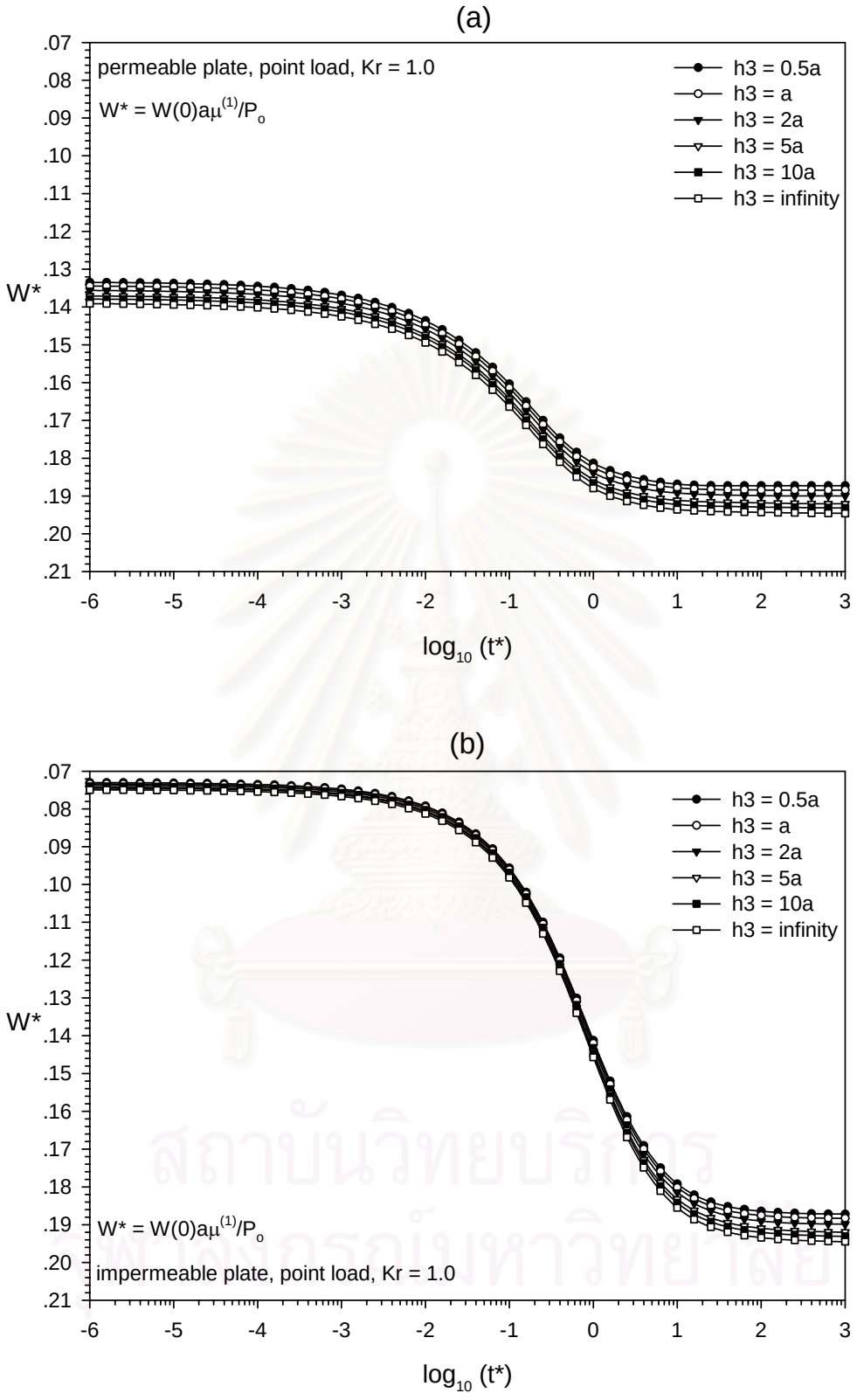

Figure 24. Variation of dimensionless central displacement W*(0) of a centrally loaded plate (K_r = 1.0) with time and depth of the 3rd layer.

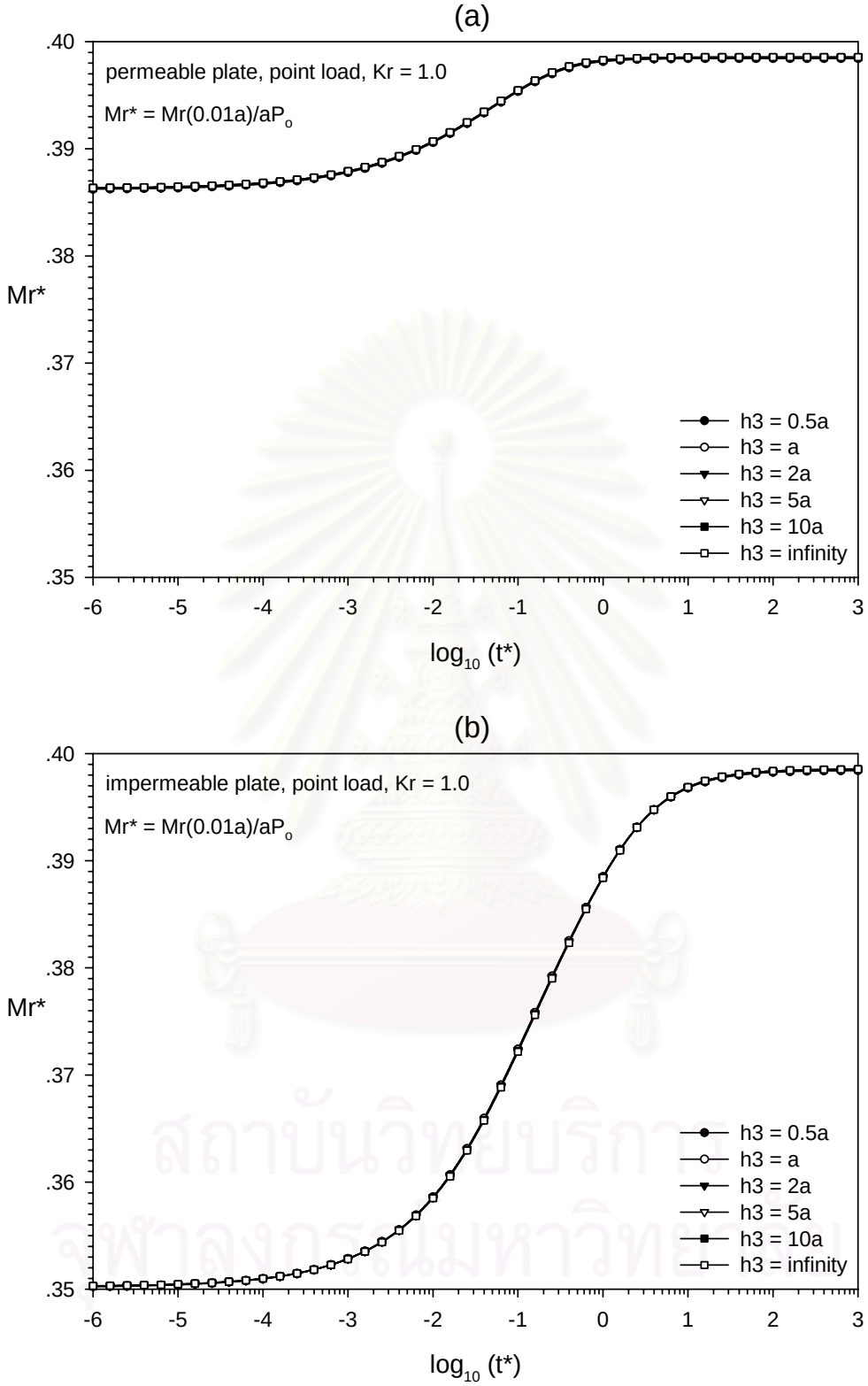

Figure 25. Variation of radial bending moment at r = 0.01a of a centrally loaded plate (K_r = 1.0) with time and depth of the 3rd layer.

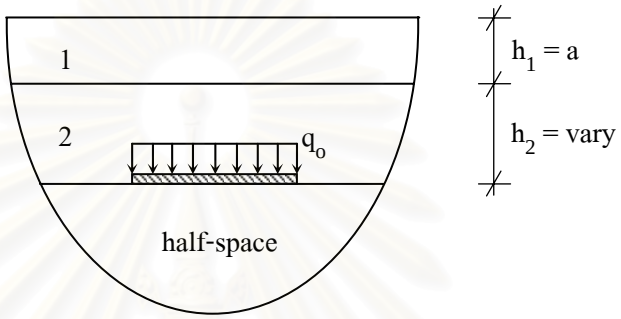

	B	ν	ν_u	$\mu^{(i)}/\mu^{(1)}$	$\kappa^{(i)}/\kappa^{(1)}$
1st layer	1.0	0.25	0.50	1	1
2nd layer	0.8	0.20	0.35	2	0.1
half-space	0.6	0.15	0.30	10	0.01

h_2 = 0.5a, a, 2a, 5a, 10a, 50a, 100a, 1000a

Figure 26. Geometry of problem 3.

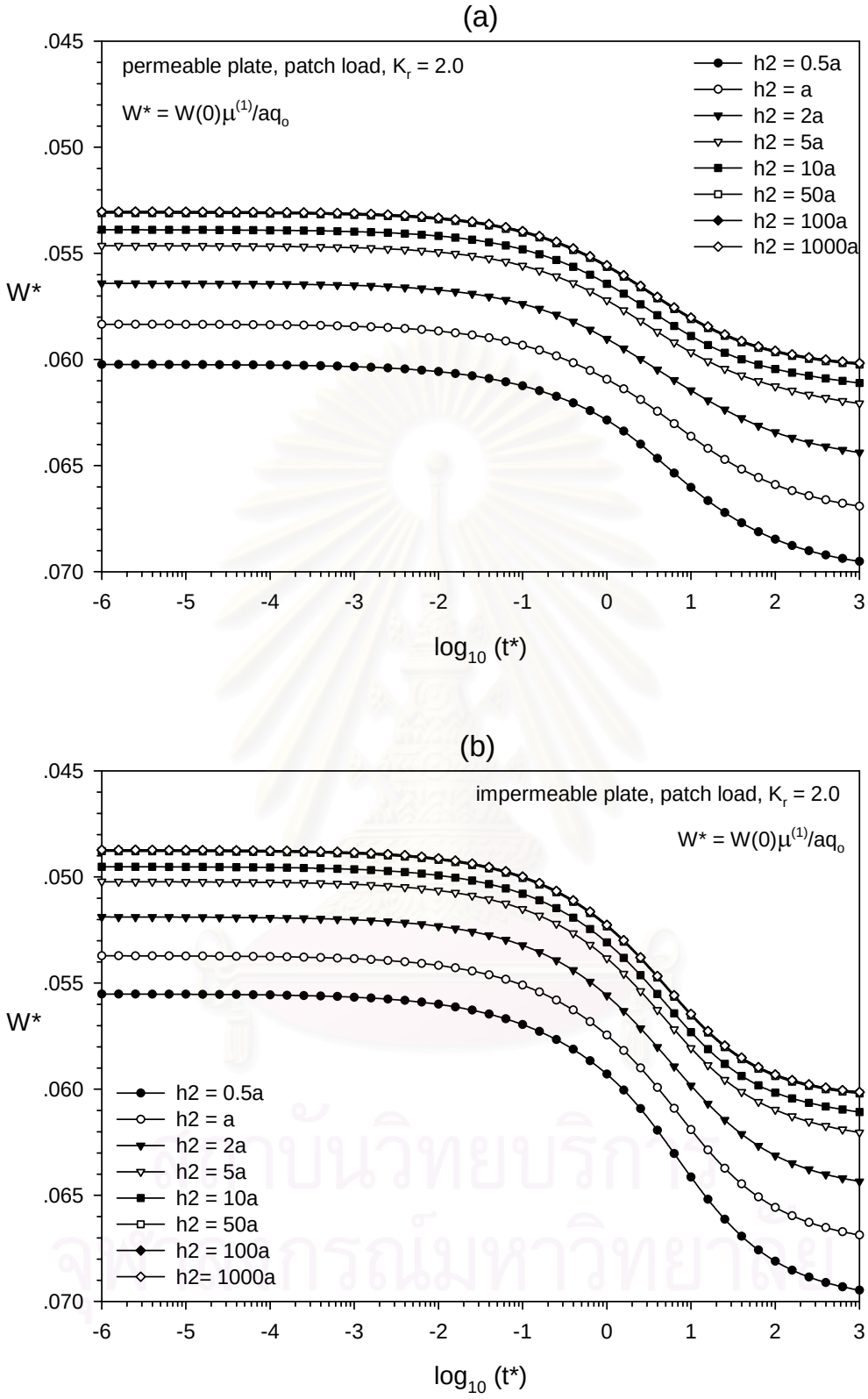

Figure 27. Variation of dimensionless central displacement of a uniformly loaded plate (K_r = 2.0) with time and thickness of the 2nd layer.

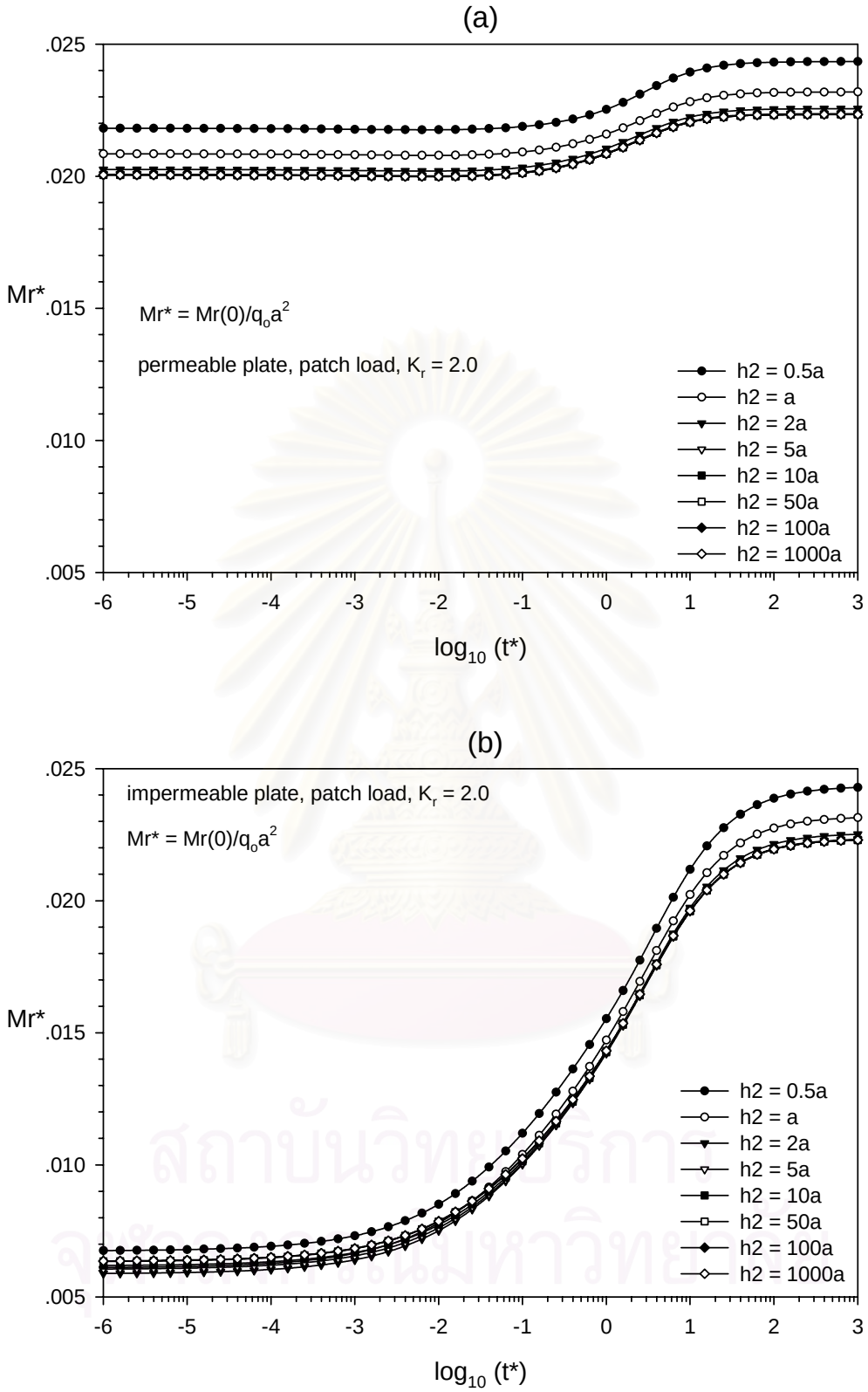

Figure 28. Variation of dimensionless radial bending moment M_r*(0) of a uniformly loaded plate (K_r = 2.0) with time and thickness of the 2nd layer.

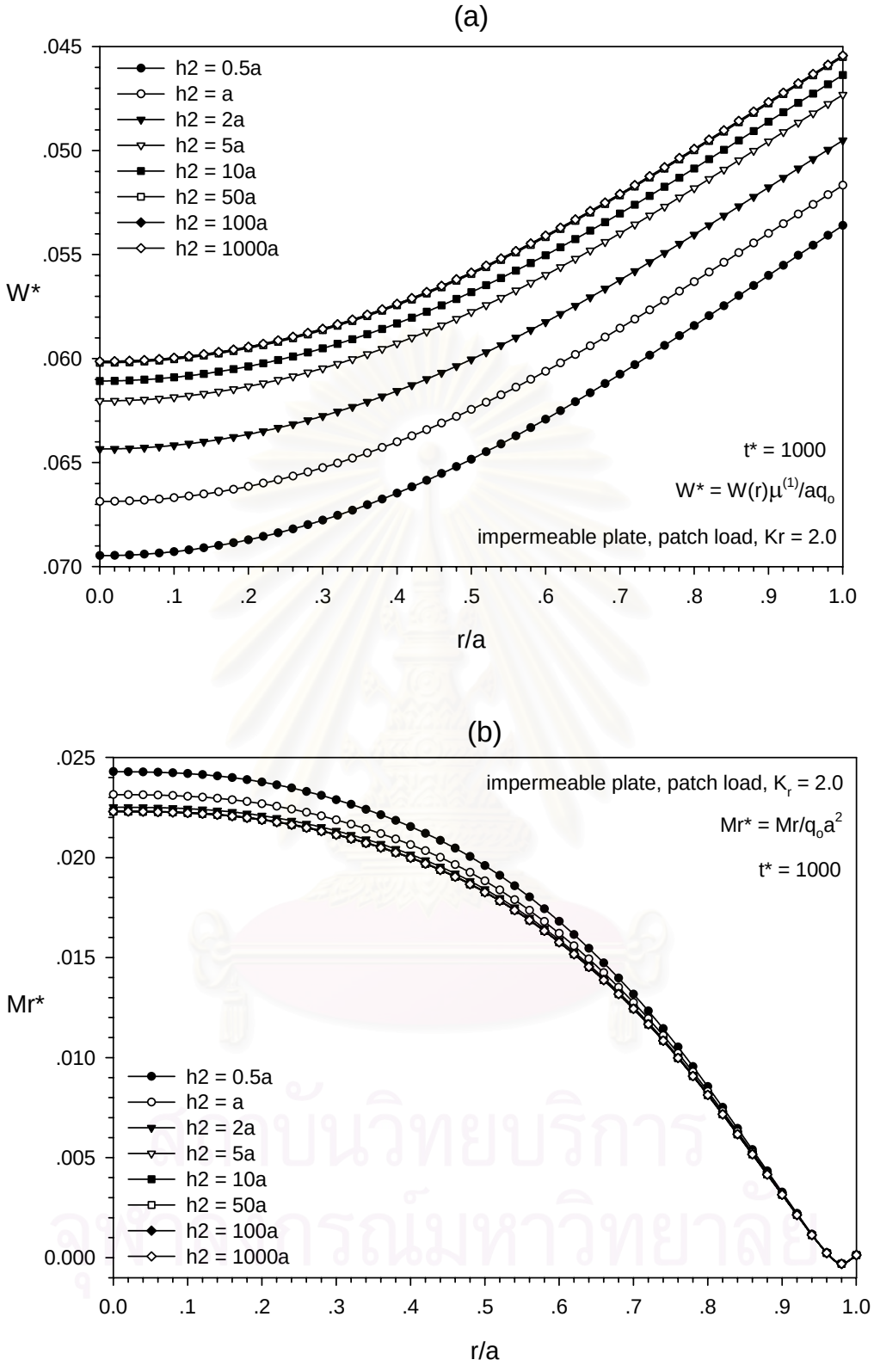

Figure 29. Variation of final solution of (a) displacement profile and (b) radial bending moment profile of a uniformly loaded plate with depth of the 2nd layer.

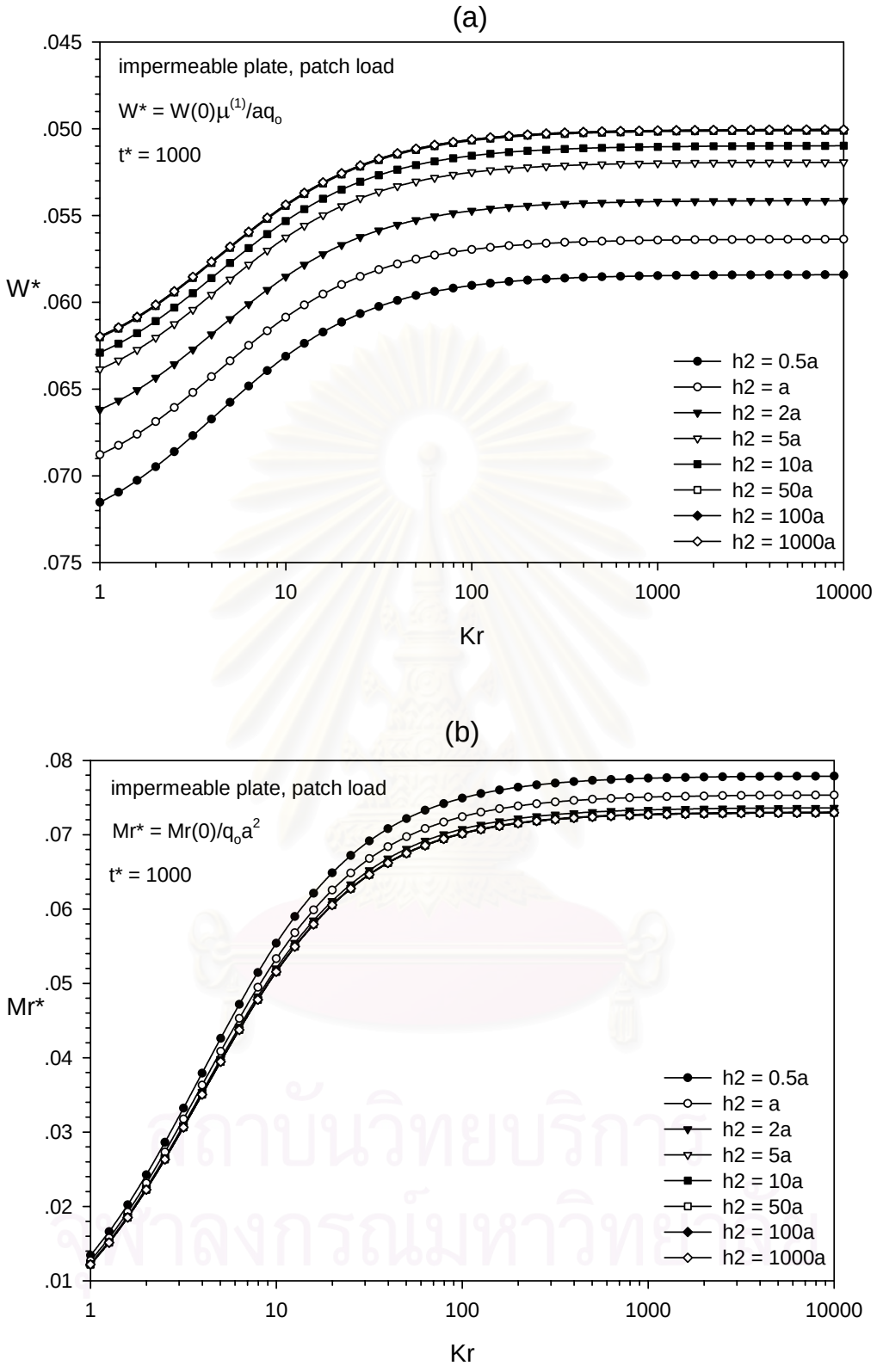

Figure 30. Variation of (a) dimensionless central displacement W*(0) and (b) dimensionless radial bending moment M_r*(0) of a uniformly loaded plate with relative rigidity parameter K_r and thickness of the 2nd layer.

REFERENCES

Agbezuge, L.K. and Deresiewicz, H. (1975), "The consolidation settlement of a circular footing", Israel Journal of Technology, 13, 264-269.

Antony, S.J. and Chandrashekhara, K. (2000), "Ring plate on a transversely isotropic elastic halfspace", A Math. Modelling, 24, 55–72.

Burmister, D.M. (1956), "Stress and displacement characteristics of a two-layer rigid base soil system : influence diagrams and practical applications", Proc. Highw. Res. Bd., 35, 773.

Butterfield, R. and Banerjee, P.K. (1971), "A rigid disc embedded in an elastic half-space", Geotech. Eng., 2, 35-53.

Biot, M.A. (1941), "General theory of three-dimensional consolidation", J. Appl. Phys., 12 , 156-164.

Biot, M.A. (1956), "General solution of the equations of elasticity and consolidation for a porous material", J. Appl. Mech., 23, 91-95.

Boussinesq, J.(1855), "Applications des Potentiels a l' Etude de l' Equillibre et du Mouvement des Solides Elastiques", Gauthier-Villars, Paris.

Brown, P.T. (1969), "Numerical analyses of uniformly loaded circular rafts on elastic layers of finite depth", Geotechnique, 19, 301–306.

Brown, P.T. (1969), "Numerical analyses of uniformly loaded circular rafts on deep elastic foundations", Geotechnique, 19, 399–404.

Carrier III, W.D. and Christian J.T. (1973), "Rigid circular plat resting on a non-homogeneous elastic half-space", Geotechnique, 23, No.1, 67-84.

Chakravorty, A.K. and Ghosh, A. (1975), “Finite difference solution for circular plates on elastic foundations”, Int. J. Numer. Meth. Eng., 9, 73–84.

Detournay, E. and Cheng, A.H.-D. (1988), “Poroelastic response of a borehole in a non-hydrostatic stress field”, Int. J. Rock Mech. Min. Sci. and Geomech. Abstr., 25, 171-182.

Fung, Y.C. (1965), Foundations of Solid Mechanics, Prentice-Hall, Englewood Cliffs, NJ.

Gibson, R.E. (1967), “Some results concerning displacements and stresses in a non-homogeneous elastic half space”, Geotechnique, 29, 461–468.

Hemsley, J.A. (1987), “Elastic solutions for axisymmetrically loaded circular raft with free or clamped edges founded on Winkler springs or a half-space”, Proc. Instn. Civ. Eng., Part 2, 83, Mar., 61-90.

Hooper, J.A. (1974), “Analysis of a circular raft in adhesive contact with a thick elastic layer”, Geotechnique, 24, 561–589.

Hooper, J.A. (1975), “Elastic settlement of a circular raft in adhesive contact with a transversely isotropic medium”, Geotechnique, 25, 691–711.

McNamee, J. and Gibson, R.E. (1960a), “Displacement functions and linear transforms applied to diffusion through porous elastic media”, Q.J. Mech. Appl. Math., 13, 98-111.

McNamee, J. and Gibson, R.E. (1960b), “Plane strain and axially symmetric problems of consolidation of a semi-infinite clay stratum”, Q.J. Mech. Appl. Math., 13, 210-227.

Melerski, E.S. (1997), “Numerical modelling of elastic interaction between circular rafts and cross-anisotropic media”, Computer & Structures, 64, No.1-4, 567-578.

Palmov, V.A. (1960), “The contact problem of a plate on an elastic foundation”, J. Appl. Math. Mech, 24, 609–618.

Pickett, G. and McCormick, F.J. (1951), “Circular and rectangular plates under lateral load and supported by and elastic solid foundation”, Proc. 1st U.S. Nat. Congress on Appl. Mech., pp. 331–338.

Piessens, R. (1975), “Bibliography on numerical inversion of the Laplace transform and application”, J. Comp. Appl. Math., 1, 115–126.

Popov, G.Y, (1971), “Plates on linearly elastic foundation (a survey)”, Soviet Appl. Mech., 8, 3–17.

Rajapakse, R.K.N.D. (1988), “The interaction between a circular elastic plate and a transversely isotropic elastic half–space”, Int. J. numer. anal. methods geomech., 12, 419–436.

Rajapakse, R.K.N.D. and Selvadurai, A.P.S. (1991), “Response of circular footings and anchor plates in non–homogeneous elastic soils”, Int. J. numer. anal. methods geomech., 15, 457–470.

Rajapakse, R.K.N.D. and Senjuntichai, T. (1993). “Fundamental solutions for a poroelastic half-space with compressible constituents”, J. Appl. Mech., 60, 844-856.

Rice, J.R. and Cleary, M.P. (1975), “Some basic stress-diffusion solutions for fluid saturated elastic porous media with compressible constituents”, Rev. Geophys. Space Phys., 14, 227–241.

Schapery, R.A. (1962), “Approximate methods of transform inversion for vicoelastic stress analysis”, Proc. 4th U.S. Nat. Congress on Appl. Mech., 2, 1075–1085.

Schiffman, R.L. and Fungaroli, A.A.(1965), “Consolidation due to tangential loads”, Proc. 6th Int. Conf. Soil Found. Eng., Montreal, Canada, 1, 188-192.

Selvadurai, A.P.S. (1979), "Elastic Analysis of Soil-Foundation Interaction", Elsevier, Amsterdam.

Senjuntichai, T. and Rajapakse, R.K.N.D. (1995), “Exact stiffness method for quasi–statics of a multi–layered poroelastic medium”, Int. J. Solids Structures, 32, 1535–1553.

Skempton, A.W. (1954), “The pore pressure coefficients A and B”, Geotechnique, 4, 143-147.

Sneddon, I.N. (1951), Fourier Transforms, McGraw-Hill, New Youk, 1951.

Stehfest, H. (1970), “Numerical inversion of Laplace transforms”, Communs. Ass. Comput. Mach., 13, 47–49.

Terzaghi, K. (1923), “Die Berechnung der Durchassigkeitsziffer des Tones aus dem Verlauf der hydrodynamischen Spannungsercheinungen”, Sitzungsber. Akad. Wiss. Wien. Math.-Naturwiss. Kl., Abt. 2A 132, 105–124.

Timoshenko, S.P. and Woinowsky-Krieger, S. (1959), Theory of Plates and Shells, McGraw-Hill, New York.

Wang, Y.H., Ni, J. and Cheung, Y.K. (2000), "Plate on non-homogeneous elastic half-space analysed by FEM", Structural Engineering and Mechanics., 9, 127-139.

Wang, Y.H. and Cheung, Y.K. (2001), “Plate on cross–anisotropic foundation analyzed by the finite element method”, Computers and Geotechnics, 28, 37–54.

Yue, Z.Q. and Selvadurai, A.P.S. (1995), “Contact problem for saturated poroelastic solid”, J. Eng. Mech., 121, 502–512.

APPENDIX

The matrices **R** and **S** in eqns (11) and (12), respectively, are given by

$$\mathbf{R} = \begin{bmatrix} -\xi\delta e^{\gamma z} & -\xi\delta e^{-\gamma z} & a_1 z e^{\xi z} & -a_1 z e^{-\xi z} & e^{\xi z} & e^{-\xi z} \\ \gamma\delta e^{\gamma z} & -\gamma\delta e^{-\gamma z} & -(a_1 z - \frac{a_2}{\xi})e^{\xi z} & -(a_1 z + \frac{a_2}{\xi})e^{-\xi z} & -e^{\xi z} & e^{-\xi z} \\ 2\mu a_3 \eta e^{\gamma z} & 2\mu a_3 \eta e^{-\gamma z} & -2\mu\eta a_4 e^{\xi z} & -2\mu\eta a_4 e^{-\xi z} & 0 & 0 \end{bmatrix} \quad \text{(A1)}$$

$$\mathbf{S} = 2\mu \begin{bmatrix} -\gamma\xi\delta e^{\gamma z} & \gamma\xi\delta e^{-\gamma z} & (a_1\xi z - \frac{1}{2})e^{\xi z} & (a_1\xi z + \frac{1}{2})e^{-\xi z} & \xi e^{\xi z} & -\xi e^{-\xi z} \\ \xi^2\delta e^{\gamma z} & \xi^2\delta e^{-\gamma z} & (a_4 - a_1\xi z)e^{\xi z} & (a_4 + a_1\xi z)e^{-\xi z} & -\xi e^{\xi z} & -\xi e^{-\xi z} \\ -a_3\kappa\gamma\frac{\delta}{c}e^{\gamma z} & a_3\kappa\gamma\frac{\delta}{c}e^{-\gamma z} & a_4\kappa\xi\frac{\delta}{c}e^{\xi z} & -a_4\kappa\xi\frac{\delta}{c}e^{-\xi z} & 0 & 0 \end{bmatrix} \quad \text{(A2)}$$

$$a_1 = \frac{1}{2(1-2\nu_u)}, \quad a_2 = \frac{(3-4\nu_u)}{2(1-2\nu_u)}, \quad a_3 = \frac{B(1+\nu_u)(1-\nu)}{3(\nu_u-\nu)}, \quad a_4 = \frac{(1-\nu_u)}{(1-2\nu_u)} \quad \text{(A3)}$$

$$\eta = \frac{B(1+\nu_u)}{3(1-\nu_u)}, \quad c = 2\mu\kappa\eta a_3, \quad \gamma = \sqrt{\xi^2 + \frac{s}{c}}, \quad \delta = \frac{\eta}{s/c} \quad \text{(A4)}$$

BIOGRAPHY

Mr. Songkran Siridejachai was born in Phitsanuloke in 1975. He graduated from Faculty of Engineering, Chulalongkorn University in 1997. He continued his education for Master Degree in Civil Engineering at Chulalongkorn University.